Modelling Estuarine Biogeochemical Dynamics: From the Local to the Global Scale

Pierre Regnier · Sandra Arndt · Nicolas Goossens · Chiara Volta ·
Goulven G. Laruelle · Ronny Lauerwald · Jens Hartmann

Abstract   Estuaries act as strong carbon and nutrient filters and are relevant contributors to the atmospheric CO_2 budget. They thus play an important, yet poorly constrained, role for global biogeochemical cycles and climate. This manuscript reviews recent developments in the modelling of estuarine biogeochemical dynamics. The first part provides an overview of the dominant physical and biogeochemical processes that control the transformations and fluxes of carbon and nutrients along the estuarine gradient. It highlights the tight links between estuarine geometry, hydrodynamics and scalar transport, as well as the role of transient and nonlinear dynamics. The most important biogeochemical processes are then discussed in the context of key biogeochemical indicators such as the net ecosystem metabolism (NEM), air–water CO_2 fluxes, nutrient-filtering capacities and element budgets. In the second part of the paper, we illustrate, on the basis of local estuarine modelling studies, the power of reaction-transport models (RTMs) in understanding and quantifying estuarine biogeochemical dynamics. We show how a combination of RTM and high-resolution data can help disentangle the complex process interplay, which underlies the estuarine NEM, carbon and nutrient fluxes, and how such approaches can provide integrated assessments of the air–water CO_2 fluxes along river–estuary–coastal zone

P. Regnier (✉) · N. Goossens · C. Volta · G. G. Laruelle · R. Lauerwald
Department of Earth and Environmental Sciences, Université Libre de Bruxelles, Brussels, Belgium
e-mail: pregnier@ulb.ac.be

S. Arndt
BRIDGE, School of Geographical Sciences, University of Bristol, Bristol, UK

R. Lauerwald
CNRS, FR636, Institut Pierre-Simon Laplace, 78280 Guyancourt Cedex, France

J. Hartmann
Institute for Biogeochemistry and Marine Chemistry, KlimaCampus, Universität Hamburg, Hamburg, Germany

continua. In addition, trends in estuarine biogeochemical dynamics across estuarine geometries and environmental scenario are explored, and the results are discussed in the context of improving the modelling of estuarine carbon and CO_2 dynamics at regional and global scales.

Keywords Reactive-transport models · Land–ocean continuum · Carbon cycle · CO_2 · Estuaries · Biogeochemistry

1 Introduction

Situated at the transition between freshwater and marine environments, estuaries are key components of the land–ocean aquatic continuum. They act as strong nutrient and carbon filters and are relevant contributors to the atmospheric CO_2 budget (e.g. Smith and Hollibaugh 1993; Cai and Wang 1998; Wollast 1998; Rabouille et al. 2001; Borges and Frankignoulle 2002; Borges 2005; Zhai et al. 2005; Laruelle et al. 2010; Borges and Abril 2011; Mackenzie et al. 2011, Laruelle et al. 2013; Regnier et al. 2013). Along the estuarine gradient, oceanic and terrestrial carbon and nutrient inputs are modified by biogeochemical processes, buried in sediments, incorporated into biomineralized structures or, in the case of gaseous species such as CO_2, exchanged with the atmosphere. All these transformations are driven by a complex interplay between geological, physical, chemical and biological processes, which are modulated by a wide array of forcing mechanisms, such as wind stress, light, water temperature, waves, tides or freshwater discharge.

The estuarine biogeochemical dynamics, the lateral carbon and nutrient fluxes and the vertical air–water gaseous exchange are characterized by strong spatial gradients from the tidally dominated mouth to the river-dominated upstream reaches. A pronounced temporal variability ranging from hours (e.g., tidal forcing) to months (e.g., discharge, seasonal temperature), and longer (e.g., historical nutrient loading) is another distinct feature of estuarine systems. Human activities, in particular, have changed both the quantity and quality of terrestrial carbon and nutrient fluxes to estuaries and the coastal ocean with likely consequences for global biogeochemical cycles and climate (Ver et al. 1999; Rabouille et al. 2001; Mackenzie et al. 2004; 2011, Regnier et al., 2013). However, the quantitative significance of the estuarine bioreactor as a regulator of land–ocean carbon and nutrient fluxes or global atmospheric CO_2 concentrations remains poorly constrained (e.g. Borges et al. 2005; Mackenzie et al. 2005; Regnier et al. 2013). This limited quantitative understanding mainly results from the inherent spatial and temporal variability of the estuarine environment that is difficult to resolve on the basis of observations alone. Observations only provide instantaneous and localized information that cannot easily be extrapolated to the scale of the entire estuarine system. Yet, important whole system properties, such as the net ecosystem metabolism (NEM, Borges and Abril 2011) and the estuarine-filtering capacity (Nixon et al. 1996), require spatially integrated assessments at a high temporal resolution over a seasonal or annual cycle (e.g. Arndt et al. 2009).

Reaction-transport models (RTMs) provide ideal tools to resolve the variability inherent in the estuarine environment. RTMs are used as analogues of the real world. Such models are based on a process–functional approach that focuses on energy and matter fluxes, and treats the biogeochemical system as a bioreactor (Haag and Kaupenjohann 2000). RTMs are generally developed to investigate the transport and transformation of a selected set of

constituents in a compartment of the Earth system. Albeit commonly used in the fields of, for example, early diagenesis or groundwater research (Lichtner et al. 1996), the concept has rarely been applied in estuarine and ocean science. Nevertheless, many biogeochemical models developed in these fields are fully consistent with the above definition.

RTMs complement field observations, because their integrative power provides the required extrapolation means for a system-scale analysis (e.g. Arndt and Regnier 2007; Arndt et al. 2009) over the entire spectrum of changing forcing conditions, including the long-term response to land-use and climate change (Paerl et al. 2006; Thieu et al. 2010). Over the last 3 decades, RTM approaches have increasingly been used to unravel the biogeochemical dynamics of estuarine systems, including studies on water quality, phytoplankton and bacterial dynamics or elemental mass budgets (e.g. O'Kane 1980; Soetaert and Herman 1995; Lee et al. 2005; Lin et al. 2007; Arndt et al. 2009; Baklouti et al. 2011; Gypens et al. 2012). Furthermore, the mechanistic understanding gained through these RTM studies allows to identify the important processes and forcings that drive the cycling of bioactive elements. They thus have the potential to provide important guidelines for the design of global biogeochemical models (e.g. Falkowski et al. 2000; Mackenzie et al. 2011). However, even today, only a few modelling studies incorporate the full suite of interacting physical, biological and chemical processes controlling the coupled transformations of carbon and nutrients along an estuarine gradient (e.g. Cloern 2001; Tappin et al. 2003; Hofmann et al. 2008a). Estuarine modelling studies are also clearly biased towards anthropogenically impacted systems in industrialized countries such as the East Coast of the USA, Western Europe and Australia (e.g. Cerco and Cole 1993; Regnier and Steefel 1999; Cerco 2000; Billen et al. 2001; Kim and Cerco 2003; Margvelashvili et al. 2003; Tappin et al. 2003; Robson and Hamilton 2004, 2008; Scavia et al. 2006; Shen 2006; Wild-Allen et al. 2009; Cerco et al. 2010). Although data availability for other regions is steadily increasing, model applications to estuaries located in Siberia, Alaska, Southeast Asia, the Hudson Bay or along the tropical Western Atlantic are missing (Fig. 1).

Our ability to assess the quantitative role of the estuarine environment for global biogeochemical cycles and greenhouse gas budgets, as well as its response to on-going land-use and climate changes, requires comparative studies that cover a large range of different systems, thus enabling the identification of global patterns (Borges and Abril 2011). However, model applications are currently limited by data requirements for calibration and validation, as well as by the high computational needs required to address physical, biogeochemical and geological processes at the relevant temporal and spatial scales. This computational barrier is rapidly exacerbated when seasonal and inter-annual timescales need to be jointly resolved. Therefore, the application of two- or three-dimensional estuarine RTMs generally remains restricted to short simulation timescales (<1 year) and well-known systems for which detailed bathymetric and geometric information is available (Fig. 1). Such two- or three-dimensional RTMs have been set up for, among others, the Chesapeake Bay (Cerco and Cole 1993; Cerco and Noel 2004; Cerco et al. 2010), the Pearl Estuary (Guan et al. 2001; Zhang and Li 2010), the St. Lawrence Estuary (Benoit et al. 2006; Lefort et al. 2012) and the Scheldt Estuary (Vanderborght et al. 2007; Arndt and Regnier 2007; Arndt et al. 2009). One-dimensional RTMs are computationally less onerous than multi-dimensional approaches. Yet, their application also remains restricted to individual estuarine systems (e.g. O'Kane 1980; Garnier et al. 1995, 2007; Hanley et al. 1998; Billen et al. 2001, 2009; Vanderborght et al. 2002; Macedo and Duarte 2006; Even et al. 2007a, b; Hofmann et al. 2008a, b), partly because regional- and global-scale simulations are currently compromised by the limited availability of comprehensive data sets. Therefore, the development of scaling approaches including new modelling tools that
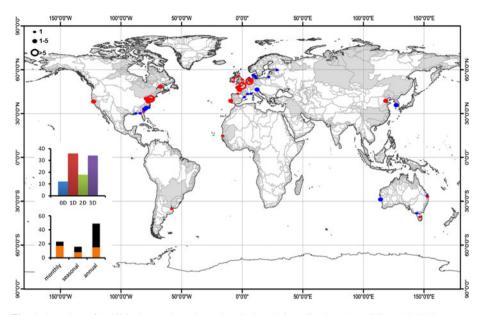
Fig. 1 Location of published estuarine biogeochemical model applications ($n = 99$). *Red*: tidal systems (type 2; $n = 74$); *Blue*: other types ($n = 25$) in the classification of Dürr et al. (2011). Watersheds highlighted in grey correspond to tidal systems. Small and big dots correspond to 1 and 1–5 model applications; circles correspond to more than 5 model applications. The bar charts represent the distribution of model dimensions (*top*) and model span (*bottom*). Steady-state (*orange*) and transient (*black*) simulations are reported separately

extrapolate knowledge from well-studied to data-poor estuarine systems is required to advance our quantitative understanding of their role in the global climate system.

In this contribution, we review the most important estuarine physical and biogeo-chemical processes that govern the transformations of carbon and nutrients along the estuarine gradient. We then illustrate, on the basis of examples of local estuarine modelling studies, how RTMs can be used to quantify estuarine budgets, fluxes and filtering capacities. The linkages and interactions between the river network, the estuarine environment and the coastal zone are also briefly analysed. Next, we show how a combination of reaction-transport modelling and high-resolution data can help disentangle the complex process interplay that underlies the estuarine NEM, greenhouse gas fluxes and C-filtering capacities. This approach is then generalized to assess the response of these key biogeochemical indicators to changes in estuarine geometry for different environmental scenarios assuming typical Western European climate conditions. Finally, the results are discussed in the context of the development of mechanistically rooted upscaling strategies, from the local to the regional scale and beyond.

2 Estuaries Within the Context of the Land–Ocean Continuum

The land–ocean aquatic continuum is commonly defined as the interface, or transition zone, between terrestrial ecosystems and the open ocean (Billen et al. 1991; Mackenzie et al. 2011; Regnier et al. 2013). Estuaries are integral part of this continuum, but their

spatial boundaries are often difficult to delineate without ambiguity (Elliott and McLusky 2002). Although estuaries may comprise coastal environments as diverse as deltas, lagoons and fjords, our analysis exclusively focuses on tidal systems due to their intense biogeochemical processing and long residence times (e.g. Wollast 1983). In addition, tidal estuaries generally reveal a sharp salinity gradient, thus facilitating model calibration and validation using specific methods that are not easily applicable to other coastal systems.

Tidal estuaries, referred to as type 2 in the typology of Dürr et al. (2011), account for a total surface area of 276 X 10^3 km^2 and 27 % of the world's exorheic freshwater water discharge (Laruelle et al. 2013). Together with large rivers, they are the main conduits through which freshwater is delivered to the sea. They also receive a significant fraction of the global carbon and nutrient load from terrestrial ecosystems. According to the analysis of the GlobalNEWS2-project (Seitzinger et al. 2005; Mayorga et al. 2010), tidal systems receive total organic carbon, nitrogen and phosphorus loads of 81, 12 and 0.7 Tg year^{-1} (an equivalent of 25, 34 and 32 % of the global land to ocean fluxes), respectively.

A tidal estuary can be geographically divided into the freshwater tidal river, the brackish to saline estuary and the area of the coastal ocean that is under the direct influence of the estuarine plume (Fig. 2). The freshwater part can often be further divided into a pre-oxygen minimum zone and an oxygen minimum zone, where a significant proportion of the terrestrial and riverine matter is processed (e.g. Vanderborght et al. 2002; Amann et al. 2012). As an example, the three major zones are illustrated in Fig. 2 for the Delaware and Scheldt watersheds. Their tidal intrusion length and thus the landward extension of the estuarine environment are highly variable as they depend on the amplitude of the tidal wave at the estuarine mouth, the estuarine geometry and the upstream river discharge. In the Delaware and Scheldt watersheds, the estuaries typically extend 170 and 215 km inwards, respectively. The average freshwater residence time is about 60–90 days in the Scheldt (Wollast and Peters 1978) and 80 days in the Delaware estuary (Fisher et al. 1988), but can vary significantly in response to changes in the freshwater discharge.

Most tidal estuaries are alluvial estuaries, which, from a morphological point of view, are geologically young environments. They are characterized by movable beds and a measurable influence of freshwater discharge. Alluvial estuaries develop in sediment deposits delivered by the river and the sea, as opposed to fixed bed estuaries, which are remnants of an older geological period. In alluvial estuaries, the tidal discharge directly depends on the channel size. In turn, the water movement, driven by the tides and the freshwater discharge, leads to a redistribution of the unconsolidated sediments, which shapes the estuary (Savenije 2005). This co-adjustment results in a dynamic equilibrium that allows deriving hydraulic information from the estuarine shape and vice versa. Thus, although alluvial estuaries cover a wide variety of shapes, their geometries reveal common characteristics (Savenije 1992). The estuarine cross-sectional area and width typically decrease exponentially with distance from the mouth. The cross-section and width convergence lengths, defined as the distance between the mouth and the point at which the cross section or width is reduced to 37 % of its value at the mouth, are directly related to the dominant hydrodynamic forcing. A high river discharge typically induces a prismatic channel with long convergence lengths, while a large tidal range results in a funnel-shaped estuary with short convergence lengths. For example, the Scheldt and the Delaware are typical tidally dominated, funnel-shaped alluvial estuaries, occasionally referred to as marine-dominated estuaries (Jiang et al. 2008), with a cross-section convergence length of only 26 and 41 km and a width convergence length of 28 and 42 km, respectively (Savenije 1992). Their width at the mouth is 15 km for the Scheldt and 38 km for the Delaware (Savenije 1992), and their average water depth is $\sim$10 m (Canuel et al. 2012).
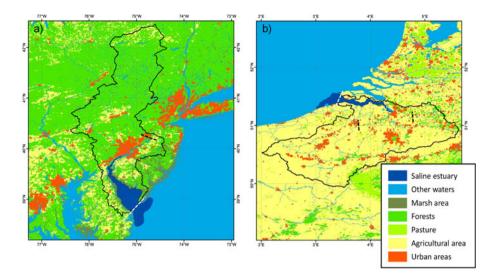
Fig. 2 The Delaware (**a**) and Scheldt (**b**) estuaries in the context of the land–ocean continuum. Black lines delineate the watersheds. White dashed line: estuarine mouth; black dashed line: upper limit of the tidal river. Land-use data were derived from the GlobCover data set (Arino et al. 2007). Information about inland water bodies and marsh areas was taken from ESRI (2006, http://www.esri.com/data/find-data) and the Corine Land Cover data set. The watersheds of the Delaware and Scheldt rivers are dominated by forests and agricultural land, respectively. Both watersheds are influenced by extensive urban areas, although their spatial distribution is contrasted. Tidal marsh areas are still abundant in the Delaware estuary, while only a single patch is present along the Scheldt estuary. Permanent web source for Corine data: http://www.eea. europa.eu

At the other end of the spectrum of shapes, the Solo or the Lalang are typical examples of fluvial-dominated, prismatic alluvial estuaries that are also referred to as river-dominated estuaries (Jiang et al. 2008). Their cross-section convergence lengths are 226 and 217 km, while their width convergence lengths are 226 and 96 km, respectively (Savenije 2005).

Within the estuarine reactor, large riverine fluxes of terrestrial or fossil dissolved and particulate organic matter mix with organic matter derived from marine sources or produced in situ (Heip and Herman 1995; Frankignoulle et al. 1998; Abril et al. 2002). This organic carbon is, together with large land-derived nutrient fluxes, biogeochemically modified along the estuarine gradient before it is ultimately exported to the adjacent coastal zone (Hedges and Keil 1999; Middelburg and Herman 2007; Arndt et al. 2011; Amann et al. 2012). At decadal scales, process rates vary due to changes in the catchment area or anthropogenic activities (e.g. Thieu et al. 2010, 2011). In a pristine watershed, for example, the major source of organic carbon is the top soil and the vegetation (Mulholland 1997; Guéguen et al. 2006; Lauerwald et al. 2012). The input of dissolved inorganic carbon, mainly carbonate alkalinity, is controlled by chemical rock weathering and thus the lithology (Meybeck 1993; Cai et al. 2008; Moosdorf et al. 2011). Land-use substantially affects carbon and nutrient exports from watersheds (Fig. 2). In agricultural areas, the application of fertilizer is the major non-point source of nutrients in surface water (Billen et al. 2009). Soil erosion plays a key role in mobilizing particulate organic carbon and phosphorus from the terrestrial to the aquatic system (Beusen et al. 2005; Quinton et al. 2010; Regnier et al. 2013). Furthermore, anthropogenic point sources of reactive nutrients and labile organic carbon can have significant effects on the biogeochemistry of rivers and

estuaries (Vanderborght et al. 2002; Mackenzie 2013). Enhanced weathering due to application of lime or rock powder to adjust soil pH causes increased alkalinity fluxes and dissolved inorganic carbon fluxes (Hartmann and Kempe 2008; Raymond et al. 2008).

3 The Estuarine Filter

3.1 Physics

The dynamic interplay between tidal forcing and freshwater inflow is the fundamental driver of estuarine hydrodynamics. It induces not only a strong spatial variability in the flow and transport properties, but also significant temporal fluctuations with characteristic timescales ranging from turbulent eddies lasting minutes to the semi-diurnal or diurnal tides, and finally the residual (long-term) circulation displaying spring–neap, seasonal and yearly cycles (O'Kane and Regnier 2003). Although the spatial and temporal aspects of the estuarine dynamics are discussed separately here, it should be emphasized that they are intimately linked.

3.1.1 Spatial Variability

The hydrodynamic and biogeochemical properties display a dominant spatial variability along the estuarine axis that is generally stronger than the cross-sectional variability (O'Kane and Regnier 2003). Because of this characteristic, a one-dimensional representation of the estuarine physics often provides a representation of the main hydrodynamic and solute transport properties that is suitable for a quantitative description of the estuarine biogeochemistry (Uncles and Radford 1980; Friedrichs and Aubrey 1988; Regnier et al. 1998).

The superposition of fluvial and tidal influences causes important longitudinal variations in energy dissipation, divergence of the energy flux, distortion of the tidal wave and salinity (e.g. Jay et al. 1990; Dalrymple et al. 1992; Arndt et al. 2007). This supports a division of the estuarine environment into a tidally dominated zone and a river-dominated zone, separated by an intermediate zone, where tidal and fluvial energy influence are of similar magnitude (Jay et al. 1990; Dalrymple et al. 1992). Figure 3 illustrates the profiles of energy dissipation, tidal amplitude and salinity along the estuarine axis. Two alluvial estuaries, characterized by a different dominant hydrodynamic forcing and, thus, different shapes, are considered: a tidally dominated, funnel-shaped estuary and a fluvial-dominated, prismatic estuary. This conceptual sketch shows that the extension of the different estuarine zones strongly depends on the relative importance of tidal and fluvial energy. A dominant tidal influence generally results in a funnel-shaped estuary that is characterized by a strong channel convergence, i.e. a short convergence length and a long salt intrusion length (Savenije 2005). In these systems, the strong convergence of the estuarine banks leads to an amplification of the tidal wave in the downstream part of the estuary where mechanical energy is almost exclusively provided by the tides. The flux divergence of the tidal energy is also balanced by dissipation at the estuarine bottom (Dyer 1995; Arndt and Regnier 2007). Energy dissipation increases in upstream direction due to channel convergence and the associated increase in tidal amplitude. The strong tidal influence counteracts the residual downstream transport of salt and maintains small salinity gradients in the lower estuary. Salinity intrudes far upstream in the estuary through dispersion and tidal pumping, and the salt intrusion length equals about two-third of the total estuarine length
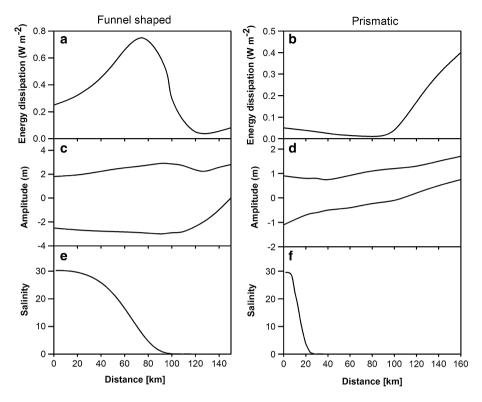
Fig. 3 Longitudinal distribution of tidal energy (**a**, **b**), tidal amplitude (**c**, **d**) and salinity (**e**, **f**) for a tidally dominated estuary (*left*) and a fluvial-dominated estuary (right)

(Savenije 2005). Further upstream, convergence becomes small, and the influence of the river discharge increases progressively. The tidal influence is significantly reduced by friction, and energy dissipation is controlled by the fluvial energy flux towards the sea (e.g. Giese and Jay 1989, Horrevoets et al. 2004). The respective areas of dominant tidal and fluvial energy dissipation are separated by a zone of minimum energy dissipation, the so-called balance point, where both contributions are of similar but low magnitude (Jay et al. 1990; Dalrymple et al. 1992). A strong fluvial influence, on the other hand, results in prismatic systems with a low channel convergence (i.e. long convergence length) and a sharp salinity gradient over a short distance. The long convergence length, as well as the dominant river discharge, results in a rapid dampening of the tidal wave upstream. Salinity decreases rapidly within the estuary because the residual downstream transport is significantly larger than the dispersive transport. Energy dissipation, on the other hand, steadily increases upstream where the dominant fluvial energy results in maximal energy dissipation (Giese and Jay 1989).

Although the spatial variability along the curvilinear axis of the estuary is generally dominant, smaller cross-sectional variability in hydrodynamics may become important for suspended particulate matter (SPM) or phytoplankton distributions, especially for systems displaying complex coastline configurations and irregular bathymetries. Such morphological features may induce significant cross-sectional and vertical gradients that cannot be resolved in a one-dimensional framework. They thus limit the quantification of processes

such as primary production (e.g. Cloern 1996, 1999), sorption onto solid particles or bottom-water hypoxia. For instance, the deep trench in the centre of the Chesapeake Bay determines the longitudinal and lateral extent of hypoxia of bottom waters during the summer (Cerco 2000). Bottom friction and wind may also induce significant vertical variations in the current field, as in the Pamlico Sound estuarine system (Lin et al. 2007). Furthermore, the benthic biogeochemical dynamics often reveal a marked two-dimensional pattern (e.g. Arndt and Regnier 2007) as a result of widely varying local hydrodynamic conditions between shallow intertidal flats, characterized by conditions of low kinetic energy and net SPM deposition, and deep tidal channels where net erosion prevails. A complex circulation is also often observed at the transition between the outer estuary and the coastal zone. Examples of such a transition zone include the Cape Fear River Estuary (e.g. Lin et al. 2008), the Seine plume (Cugier et al. 2005), the Scheldt Estuary (Arndt et al. 2011), the Chesapeake Bay (Cerco 2000) or the Bay of Brest (Laruelle et al. 2009a).

3.1.2 Temporal Variability

Estuaries are inherently dynamic systems that are characterized by nonlinearities in flow and material transport, as well as important departures from steady state (e.g. Regnier et al. 1997; Uncles and Stephens 1999; Dyer 2001; Arndt et al. 2009). The transient nature of the estuarine environment can be illustrated by examining the relationship between salinity and river discharge (Fig. 4a). If the estuary is in a time-invariant state, the seaward advection of salt exactly balances the landward dispersion of salt (Bowden 1963). In this case, the river discharge unambiguously determines the salinity for any given cross section along the estuarine gradient (Regnier et al. 1998). Therefore, differences between observed pairs of river–discharge–salinity values and the theoretical steady-state relationship (solid curve in Fig. 4a) serve as a 'measure' of the departure from steady state (e.g. Officer and Lynch 1981). For a passive tracer, the time required for the estuarine system to adjust to fluctuating boundary conditions (weeks to months) is much larger than the characteristic timescales of these fluctuations (days to a few weeks). The resulting time lags create the observed departures from steady state (Fig. 4a) and can lead to a significant transient mass storage (or depletion) within the estuary. This is also true for reactive species, for which the interplay between transient mass storage and production/consumption processes can lead to complex seasonal dynamics (see, for instance, Sect. 4.2.1 and Fig. 7).

The generation of low-frequency components by nonlinear interactions among tidal constituents also leads to significant fluctuations in the residual (long-term) water flow. This effect can be of sufficient magnitude and persistence to exert a significant influence on the residence time and, thus, on the biogeochemical transformations within the estuary (e.g. Regnier et al. 1998; Arndt et al. 2009). The relative magnitude of these nonlinear interactions depends on the physical characteristics of the estuary and the external forcings (Parker 1991). Figure 4b illustrates snapshots of the departure of the residual cross-sectional water flow from the mean river discharge along the gradient of a macro-tidal estuary for different discharge conditions. The difference between residual water flow and mean river discharge is maximal close to the estuarine mouth and decreases with an increase in fluvial influence upstream. Although the difference is most pronounced under low to average discharge conditions, it is still noticeable under high discharge conditions. The tidally induced fluctuations in the residual transport field can even result in a landward residual water flow if low river discharge coincides with a spring tide (Regnier et al. 1998). Such dynamics have been reported for numerous estuaries (e.g. Uncles and Jordan 1980;
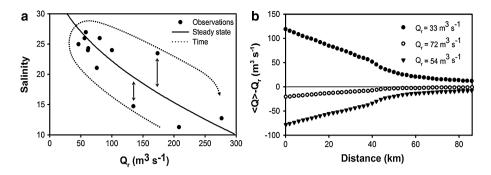
Fig. 4 **a** Salinities at a fixed location along the longitudinal curvilinear axis of a macrotidal estuary (the Scheldt, BE-NL) as a function of freshwater river discharge Q_r. The *solid line* is the theoretical Q_r-S curve for an estuary at steady state. The thin arrow represents the observed yearly time evolution path. The *double arrows* indicate departure from steady state. **b** Longitudinal distribution of the residual water flow ($< Q > - Q_r$) computed at different times of the year for different river discharges. $< Q >$ is the tidally averaged water flux through a given cross section. Modified from Regnier et al. (1998)

Sommerfield and Wong 2011) and have important implications for the quantification of biogeochemical processes and export fluxes of C and nutrients.
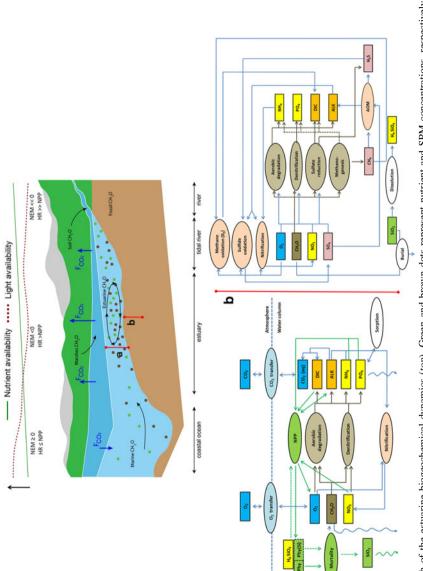
3.2 Biogeochemistry

The most important biogeochemical processes that determine estuarine biogeochemical dynamics are represented schematically in Fig. 5. Here, their significance for key biogeochemical indicators (NEM, estuarine carbon dioxide fluxes and nutrient-filtering capacity) and elemental budgets is discussed.
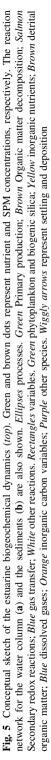
3.2.1 Biogeochemical Processes

Organic matter (CH_2O in Fig. 5) plays a key role in the biogeochemical dynamics of estuarine systems, because the production and degradation of organic carbon exert an important influence on almost all biogeochemical variables. Estuaries receive a complex mix of organic matter from very different sources as reflected by their characteristic $\delta^{13}C$ and $\Delta^{14}C$ profiles between the river and marine end-members (e.g. Middelburg and Herman 2007). Large amounts of allochthonous terrestrial or fossil organic matter are exported from land by rivers and groundwater. In addition, rivers may carry significant amounts of labile organic matter from anthropogenic sources, for instance, sewage (Mackenzie et al. 2011). Along the estuarine gradient, this allochthonous organic matter is mixed with autochthonous organic matter produced by phytoplankton or intertidal vegetation and, further downstream, with allochthonous marine organic matter imported from the coastal ocean through tidal pumping (Bianchi 2007). While the amount of allochthonous material brought into the estuary is essentially controlled by transport, the contribution of autochthonous material to the estuarine organic matter pool is determined by the difference between rates of net primary production (NPP), phytoplankton (Phy) mortality and subsequent decomposition (Fig. 5).

In estuarine environments, NPP strongly depends on the interplay between water column turbidity, nutrient availability and the flushing rate of estuarine waters that control the residence time of phytoplankton in the system (Cloern et al. 1983). In addition,

Fig. 5 Conceptual sketch of the estuarine biogeochemical dynamics (*top*). Green and brown dots represent nutrient and SPM concentrations, respectively. The reaction network for the water column (**a**) and the sediments (**b**) are also shown. *Ellipses* processes. *Green* Primary production; *Brown* Organic matter decomposition; *Salmon* Secondary redox reactions; *Blue* gas transfer; *White* other reactions. *Rectangles* variables. *Green* phytoplankton and biogenic silica; *Yellow* inorganic nutrients; *Brown* detrital organic matter; *Blue* dissolved gases; *Orange* inorganic carbon variables; *Purple* other species. *Wiggly arrows* represent settling and deposition

phytoplankton generally suffers from osmotic stress upon exposure to salinity change, resulting in a characteristic transition from stenohaline freshwater to mesohaline and euryhaline marine phytoplankton groups along the estuarine salinity gradient (e.g. Lionard et al. 2005; Muylaert et al. 2009; Lancelot and Muylaert 2011). In polluted estuaries that are subject to high nutrient loads, turbidity and residence time are the dominant controls on NPP (Gattuso et al. 1998; Cloern 1999; Desmit et al. 2005; Gazeau et al. 2005; Arndt et al. 2007). An accurate description of NPP therefore requires quantification of the in situ light availability and phytoplankton growth parameters specific for light-limited systems (Harding et al. 1986; Langdon 1988; Lancelot et al. 1991, Lewitus and Kana 1995; Lancelot et al. 2000; Desmit et al. 2005). Estuarine NPP rates determine the relative contribution of autochthonous organic matter to the estuarine C budget, but also the extent to which the dissolved inorganic nutrient pools of phosphate (PO_4^{3-}), nitrogen (DIN = NH_4^+ +NO_3^- +NO_2^-) and silica (H_4SiO_4) are consumed (Fig. 5). In diatom-dominated estuaries, subject to high PO_4^{3-} and DIN loadings, H_4SiO_4 is often the limiting nutrient and a complete consumption during the phytoplankton bloom may occur (Arndt et al. 2007). In addition, NPP fixes dissolved inorganic carbon (DIC), produces oxygen (O_2) and impacts the exchange fluxes of estuarine gases through the air–water interface. It also exerts a complex influence on the alkalinity (Alk) budgets with opposite effects depending on whether NH_4^+ or NO_3^- is the preferential N source (Table 1).

A fraction of detrital organic matter of variable stoichiometric Redfield ratio is degraded by microbial activity during estuarine transit, thereby releasing various amounts of inorganic nutrients, DIC and alkalinity (Fig. 5; Table 1). The rate of heterotrophic degradation strongly depends on the reactivity of the organic matter (Arndt et al. 2013). The complex mix of allochthonous and autochthonous organic carbon compounds contains myriad structural motifs and functional groups covering a large range of degradabilities. With the exception of labile fresh anthropogenic DOC, terrestrial organic matter is generally less reactive than algal organic matter (e.g. Hedges et al. 2000) due to (i) a chemical composition dominated by moderately resistant (e.g. cellulose, lignin and cutin) or highly resistant (e.g. cutan) biopolymers (de Leeuw and Largeau 1993), (ii) pre-ageing during burial in soils and subsequent transport and/or (iii) protection via associations with minerals or other organic matter (e.g. Bianchi 2011). In addition, deposition/erosion cycles and redox oscillations characteristic of estuaries (Abril et al. 2000) may induce a repartitioning of organic matter between particulate and dissolved phases, which affects the composition and degradability of organic matter (Keil et al. 1997; Hedges and Keil 1999). This complexity in organic matter composition and reactivity is currently poorly represented in estuarine biogeochemical models and constitutes a serious limitation for diagnostic and prognostic analyses, especially in poorly surveyed estuarine systems.

Heterotrophic degradation often results in a characteristic redox zonation of the estuarine waters (e.g. Billen 1975; Wollast and Peters 1978; Wollast 1983; Regnier et al. 1997; Eyre and Balls 1999; Eyre 2000; Heip and Herman 1995; Bianchi 2007). In particular, in estuaries that are subject to high riverine organic matter inputs, high aerobic respiration rates may exceed the uptake capacity for atmospheric oxygen, resulting in anoxic conditions in some portions of the water column and high denitrification rates (Officer et al. 1984; Paerl et al. 1998; Rabalais and Turner 2001). If nitrate becomes a limiting reactant for organic matter degradation, other anaerobic pathways such as methanogenesis or sulphate reduction may be initiated (Thullner et al. 2007). However, these pathways are generally quantitatively significant only for organic matter degradation in estuarine sediments where oxygen is rapidly depleted within the first few centimetres (Fig. 5, Pallud and Van Cappelen 2006). Downstream, an intensification of mixing processes improves water

Table 1 Stoichiometry of the biogeochemical reactions influencing the estuarine C dynamics

	Reaction stoichiometry	CH_2O	Phy	DIC	Alk
FCO_2	$CO_2(aq) \leftrightarrow CO_2'$			$\pm1^*$	0
NPP_{NO3}	$106CO_2 + 122H_2O + 16NO_3^- + HPO_4^{2-} + 18H^+ \xrightarrow{h\nu} Phy + 138O_2$		+1	−1	+17/106**
NPP_{NH4}	$92CO_2 + 92H_2O + 16NH_4^+ + 14HCO_3^- + HPO_4^{2-} \xrightarrow{h\nu} Phy + 106O_2$		+1	−1	−15/106**
Aerobic degradation	$CH_2O + 106O_2 \longrightarrow 92CO_2 + 14HCO_3^- + 16NH_4^+ + HPO_4^{2-} + 92H_2O$	−1		+1	+15/106**
Denitrification	$CH_2O + 94.4NO_3^- \longrightarrow 55.2N_2 + 92.4HCO_3^- + 13.6CO_2 + HPO_4^{2-} + 84.8H_2O$	−1		+1	+93.4/106**
Nitrification	$NH_4^+ + 2O_2 \longrightarrow NO_3^- + 2H^+ + H_2O$			0***	−2***
Mortality	$Phy \longrightarrow CH_2O$	+1	−1	0	0

All stoichiometric coefficients are given per mole of C reacted, except for the nitrification reaction. Phy and CH_2O denote living phytoplankton and detrital organic matter, respectively. Both are assumed to have the stoichiometric ratio $(CH_2O)_{106} (NH_3)_{16} (H_3PO_4)$

* Depends on the direction of the flux (+: dissolution; −: outgassing), ** assuming Redfield stoichiometric ratio, *** per mole of N oxidized

column oxygenation and ultimately results in fully oxic conditions. Nitrification is another major process in polluted estuaries subject to large ammonium loads originating mainly from sewage discharge (Billen 1975). It exerts a strong control not only on the O_2 balance and N speciation (Fig. 5), but also on the alkalinity and pH of estuarine waters (e.g. Regnier et al. 1997; Dai et al. 2006; Hofmann et al. 2008b). Therefore, nitrification needs to be accounted for in the estuarine greenhouse gas dynamics. The rates of ammonium oxidation have been extensively studied in the laboratory and in the field (e.g. Billen 1975; Brion and Billen 1998; Soetaert et al. 2006; Dai et al. 2008) and reveal a complex seasonal pattern attributed to the growth of the chemoautotrophic bacteria sustaining their metabolic needs by catalysing this redox reaction.

Gas exchange at the air–estuarine water interface controls not only the dissolved O_2 level, but also DIC concentrations and, thus, the entire inorganic carbon system of estuaries (Fig. 5). The exchange rate is determined by the gas concentration gradient at the interface (see e.g. Weiss and Price 1980; Benson and Krause 1984) and the piston velocity, which is a function of the current velocity (O'Connor and Dobbins 1956; Vanderborght et al. 2002; Borges et al. 2004) and wind speed (Wanninkhof 1992; Raymond and Cole 2001, Regnier et al. 2002). The respective contribution of these two terms remains nevertheless difficult to assess (Vanderborght et al. 2002; Alin et al. 2011).

A fraction of the pelagic organic matter is subject to sedimentation and deposition on the estuarine floor. The benthic degradation of organic matter (Fig. 5) releases DIC, alkalinity, NH_4 and PO_4 to the water column. It also drives a downward flux of oxidants (e.g. O_2, NO_3, SO_4) that are directly consumed either by organic matter degradation or by re-oxidation reactions of reduced compounds (e.g. Van Cappellen and Wang 1996; Regnier et al. 2011) produced in situ within the sediments (e.g. NH_4, CH_4). A fraction of the deposited organic matter may nevertheless escape decomposition, and sediments are preferential places for C, N and P burial. Inorganic phosphorus removal can also occur through sorption and settling of Fe(III) oxides and other solid particles (e.g. Krom and Berner 1980; Frossard et al. 1995; van der Zee et al. 2007; Spiteri et al. 2008). It can also remain trapped in the form of highly insoluble Fe-phosphate minerals (Compton et al. 2000; Paytan and McLaughlin 2007).

Similarly, the benthic dissolution of biogenic silica originating from settling of diatom blooms may represent an important pathway in the estuarine silica cycle (e.g. Struyf et al. 2005). Through mechanisms of physical protection, some of the deposited biogenic silica can also be preserved in sediments (Qin and Weng 2006). Estuarine sediments could thus be important modifiers of the fluxes of nutrients from land to ocean (Billen et al. 1991; Howarth et al. 1995; Tappin 2002). It is, however, important to acknowledge that the global-scale burial of C, N, P and Si in estuarine systems remains largely unknown (Rabouille et al. 2001; Laruelle et al. 2009b; Regnier et al. 2013).

3.2.2 Estuarine Biogeochemical Indicators

Biogeochemical indicators are integrative measures of the biogeochemical dynamics. While most water quality indicators such as nutrient thresholds or the development of toxic algae blooms only consider specific system attributes, a system-based, holistic approach relying on a categorization of the estuarine biogeochemical dynamics in terms of NEM, carbon- and nutrient-filtering capacities and carbon dioxide fluxes (FCO_2) is proposed here.
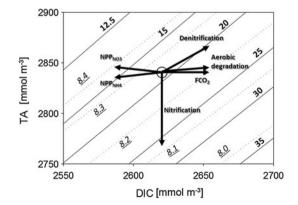
The NEM represents a biogeochemical indicator of the estuarine trophic status (Odum 1956). It is defined as the difference between net primary production (NPP) and total heterotrophic respiration (HR) on a system scale (e.g. Andersson and Mackenzie 2004). It

is therefore controlled by the production and decomposition of autochthonous organic matter, by the amount and degradability of organic carbon delivered by rivers and by the export of terrestrial and in situ produced organic matter to the adjacent coastal zone. Following the definition of NEM, the trophic status of estuaries can be net heterotrophic (NEM < 0) when HR exceeds NPP or net autotrophic (NEM > 0) and when NPP is larger than HR because the burial and export of autochthonous organic matter exceeds the decomposition of river-borne material. A recent synthesis by Borges and Abril (2011) reveals that out of the 79 estuaries investigated, 66 (84 %) have a NEM < 0. The net heterotrophic character of estuaries (Fig. 5) is largely related to high allochthonous organic matter inputs and their high turbidity, which limits NPP despite significant nutrient loads from the watersheds (Heip and Herman 1995, Gazeau et al. 2004, 2005). Nevertheless, autotrophic processes progressively gain in importance in downstream direction, and estuaries become less heterotrophic (Fig. 5). In the coastal ocean, primary production may exceed respiration and net autotrophy can prevail in this portion of the land–ocean continuum (e.g. Gattuso et al. 1998; Rabouille et al. 2001; Chen et al. 2003; Ducklow and McAllister 2004).

The balance between autotrophic and heterotrophic processes controls to a large degree the inorganic carbon cycle and, thus, the exchange flux of CO_2 through the air–water interface. As detailed in Table 1, biogeochemical processes influence both the dissolved inorganic carbon (DIC) and alkalinity (Alk) budgets. The resulting speciation of inorganic carbon species and pH as well as the air–water flux of CO_2 can be solved using, e.g. the standard approach proposed by Follows et al. (2006). These effects are represented schematically in Fig. 6 for typical estuarine conditions (Zeebe and Wolf-Gladrow 2001).

Aerobic degradation releases significant amounts of DIC but does not change significantly the Alk of the water (δAlk/δDIC = 15/106). Therefore, the δDIC and δCO_2 induced by this process are quite similar. Denitrification releases almost as much Alk than DIC (δAlk/δDIC = 93.4/106) and consequently exerts a marked buffering effect on the CO_2 concentration, with a limited change in δCO_2 per mole of DIC released. Nitrification decreases Alk without DIC change and shifts the inorganic carbon speciation towards CO_2 (δAlk/δDIC = −2/0). This process leads to a pH drop that favours a CO_2 loss towards the atmosphere. NPP using NO_3 as the N source has a higher buffering efficiency than NPP using NH_4, although both pathways promote a pH rise and limit CO_2 evasion (Soetaert et al. 2006). Therefore, the CO_2 outgassing can conveniently be decomposed as a sum of three terms associated with (1) NEM = NPP − HR, (2) the fraction of the CO_2 brought

Fig. 6 Effect of biogeochemical processes on DIC and TA. Solid lines indicate levels of constant $[CO_2]$ (in mmol m^{-3}), and *dotted lines* indicate levels of constant pH. Those results are presented for a salinity of 15 and a temperature of 17 °C. Stoichiometric equations related to each process are given in Table 1

into the estuary by supersaturated river waters that is outgassed during estuarine transit and (3) CO_2 produced through a shift in speciation induced by nitrification (Regnier et al. 1997; Frankignoulle et al. 1998; Vanderborght et al. 2002; Borges and Abril 2011). The NEM contribution can further be decomposed into its component fluxes (aerobic respiration, denitrification, NPP).

It should be noted that carbonate precipitation ($\delta Alk/\delta DIC = -2/-1$) and dissolution ($\delta Alk/\delta DIC = 2/1$) may also influence the inorganic carbon balance, respectively, in favour and against a CO_2 transfer towards the atmosphere. For instance, it has been shown that the Net Ecosystem Calcification (NEC, defined as the difference between calcification and carbonate dissolution) contributes to the CO_2 evasion of many shallow tropical estuarine systems where benthic calcification is significant (Andersson and Mackenzie 2004). Nevertheless, it is very likely that the NEM largely dominates the inorganic carbon balance in most temperate land–ocean transition systems (Borges and Abril 2011).

The estuarine-filtering capacity is another important Estuarine Biogeochemical Indicator and is a dimensionless number defined as the ratio of the net consumption of a specific element integrated over the entire estuarine domain during a given time interval to its total input (e.g. Nixon et al. 1996; Dettman 2001; Arndt et al. 2009; 2011). Reported DIN-filtering capacities range from values as low as 0.01–0.1 (Nielsen et al. 1995; Nedwell and Trimmer 1996; Nowicki et al. 1997; Trimmer et al. 1998; Mortazavi et al. 2000; Eyre and McKee 2002; Arndt et al. 2009) to values larger than 0.5 (Seitzinger 1988; Wulff et al. 1990; Boynton et al. 1995). Intermediate conditions, in the range 0.1–0.5, have also been reported (Nixon et al. 1996; van Beusekom and de Jonge 1998; Arndt et al. 2009). The retention of silica in estuaries has been much less studied, but the few reported filtering capacities range between 0 and 0.4 (DeMaster 1981; Aston 1983; Conley 1997; Arndt et al. 2009). Surprisingly, the estuarine-filtering capacity with respect to carbon has not been formally investigated.

The filtering capacity is usually defined for a specific element irrespective of its chemical form, e.g. total carbon made of the sum of inorganic and organic carbon species, both in the dissolved and in the particulate phases. Using this definition, the long-term filtering capacity (annual to decadal timescales) can then be attributed to the exchange of matter through the material surfaces of the estuary (loss to the air by outgassing or loss through burial). On shorter, seasonal timescales, the filtering capacity may also be influenced by transient mass accumulations within the estuary (e.g. Regnier and Steefel 1999; Arndt et al. 2009).

4 Quantifying the Estuarine Filter

4.1 Data-Driven Approaches and Box Models

Property-salinity plots have been widely used to estimate the export fluxes of carbon and nutrients from estuarine systems (see e.g. Stommel 1953; Ketchum 1955; Boyle et al. 1974; Pritchard 1974; Liss 1976; Wollast and Peters 1978; Officer 1980; Kaul and Froelich 1984; Mills and Quinn 1984; Billen et al. 1985; Keeney-Kennicutt and Presley 1986; GESAMP 1987; Yeats 1993; Shiller 1996; Cai and Wang 1998; Cai et al. 2004). This so-called apparent zero end-member (AZE) method builds on the assumption that mixing two water masses of different salinities results in a linear distribution of conservative species along the salinity gradient (e.g. Boyle et al. 1974; Officer and Lynch 1981). Based on this assumption, net export fluxes can then be calculated by extrapolating concentrations measured in the saline part of the estuary to the point of zero salinity. The intercept of the

regression (the apparent zero end-member concentration, AZE) multiplied by the river discharge gives an estimate of the export flux for a reactive constituent. Estimates derived using the AZE method can only account for biogeochemical transformations within the saline part of the estuary and, therefore, ignore any processing taking place in the tidal river (Vanderborght et al. 2002; Amann et al. 2012). Numerous studies have also highlighted that the AZE technique introduces large errors in the estimation of the long-term residual constituent flux towards the coastal zone (e.g. Boyle et al. 1974; Officer and Lynch 1981; Kaul and Froelich 1984; Regnier et al. 1998; Webster et al. 2000). However, the most important impediment to its application is the inherently transient nature of estuarine systems that results in nonlinear mixing curves (see Sect. 3.1). This limitation applies to the full spectrum of estuaries, from those having short residence times of days to those exhibiting much longer residence times of weeks to months.
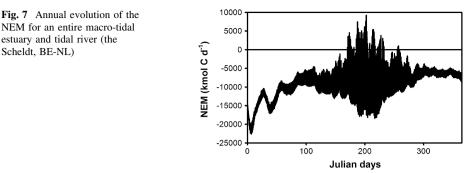
Box models have been used as an alternative approach, amenable for non-steady-state conditions (Schroeder 1997; Garnier et al. 2008; Wulff et al. 2011). Box models treat the estuary as a single, vertically and horizontally well-mixed box with steady residual hydrodynamic characteristics. The use of box models to quantify carbon and nutrient cycling in estuarine systems was made particularly popular by the LOICZ program (Gordon et al. 1996). However, studies have shown that the use of time-averaged concentrations, the assumptions of a well-mixed box and steady-state residual flow may result in large errors in estimates of estuarine transformation rates and export fluxes (e.g. Regnier et al. 1998; Webster et al. 2000; Arndt et al. 2009). For instance, Webster et al. (2000) showed that internal production from a distributed source is underestimated by a factor of two if the estuary is treated as a well-mixed box. In general, the errors depend on estuary's mixing and geometrical characteristic as well as on the location of the source. The box model approach is also very difficult to apply to estuaries characterized by high average salinities, because it scales the net export to a horizontal gradient that is highly uncertain. Therefore, reliable carbon and nutrient flux estimates call for methods that can account for the strong spatial and temporal variability of the estuarine environment.

4.2 Reaction-Transport Models

4.2.1 Spatial–Temporal Variability: Models as Integration Tools

RTMs are, in combination with observational data, ideal tools to investigate and quantify process rates, material fluxes and budgets at spatial and temporal scales that are not readily accessible through observations.

As an example, Fig. 7 illustrates the simulated annual evolution of the NEM in a macrotidal estuary. A quantitative assessment of this annual evolution would be difficult, if not impossible, on the basis of observations alone, since the NEM is an integrative measure of the whole system biogeochemical dynamics and reveals a significant temporal variability ranging from the hourly to the seasonal timescale (Fig. 7). It is thus not a directly observable quantity. Simulation results show that the NEM is negative throughout most of the year, reflecting the dominant contribution of heterotrophic processes, a common characteristic feature of many estuarine environments (Borges and Abril 2011). In particular, during winter, high heterotrophic process rates are sustained by large inputs of allochthonous organic material. During the summer months, an increase in ambient temperature supports high heterotrophic rates and maintains a mean, negative NEM. However, a simultaneous increase in primary productivity leads to a complex balance between autotrophic and heterotrophic processes that is reflected in large, short-term NEM

Fig. 7 Annual evolution of the NEM for an entire macro-tidal estuary and tidal river (the Scheldt, BE-NL)

fluctuations. The estuary may even become net autotrophic (NEM > 0) when low SPM concentrations in combination with high solar radiation increase the in situ light availability and, thus, promote high net primary production rates that exceed heterotrophic degradation rates.

Similar to the NEM, estuarine mass inventories and export fluxes are spatially integrative measures of a complex process interplay (Arndt et al. 2009, 2011). In particular, the estuarine–coastal ocean interface is characterized by instantaneous fluxes that are orders of magnitude larger than the residual flux and comprise a strong dispersive component flux (Regnier and Steefel 1999; Arndt et al. 2011). Therefore, the quantification of carbon and nutrients export is hardly achievable with observational means alone.

Figure 8 illustrates the simulated annual evolution of the estuarine silica mass budget in a macro-tidal estuary (Arndt et al. 2009). It shows the residual silica input and output fluxes across the estuarine interfaces (Fig. 8a, d, respectively), the mass of silica within the estuary (Fig. 8b), and the spatially integrated consumption rate of silica (Fig. 8c). The large intra-annual variability in the silica inventory and flux is an incitement to establish an estuarine silica budget at the biogeochemically relevant seasonal timescale (Fig. 8e). Simulation results highlight the transient nature of the silica dynamics and the critical role of changes in the silica mass inventory. Large seasonal changes (Fig. 8b) are caused by the transient nature of the mass transport, as well as by the nonlinearity in instantaneous and residual flows (see Sect. 3.1). In winter and autumn, high discharge periods trigger an increase in the storage of silica within the estuary (Fig. 8a, b). The stored silica is then progressively released during spring and summer, resulting in a depletion of the estuarine silica inventory (Fig. 8b, e). In addition, silica consumption further depletes the silica pool in summer (Fig. 8c, e). As a consequence, the filtering capacity of the system increases from close to zero in winter to 0.81 in summer. The build-up of the silica inventory and its delayed release has important implication for silica export fluxes to the coastal ocean. In particular, the export flux is characterized by a damped and smeared response to the winter fluctuations in input flux, resulting in a significant imbalance between input and output fluxes (Fig. 8d).

The quantitative assessment of the estuarine carbon and nutrient fluxes is further complicated by the complex interplay of estuarine and coastal processes at the transition between these two environments (e.g. Arndt et al. 2011). Because the separation between estuarine and coastal research has largely been based on the geographical criteria, estuarine models have generally neglected the marine influence. A fully transient simulation of the entire mixing zone of the estuary–coastal zone continuum of the Scheldt (Arndt et al. 2011) suggests nevertheless that the estuarine–coastal zone interface may play a significant role
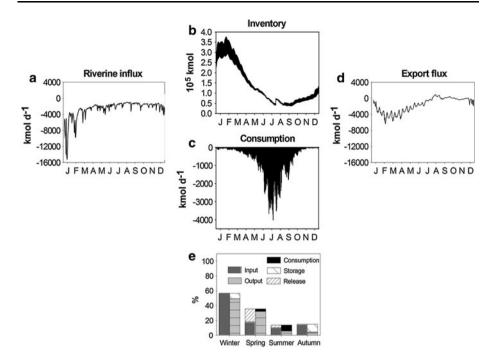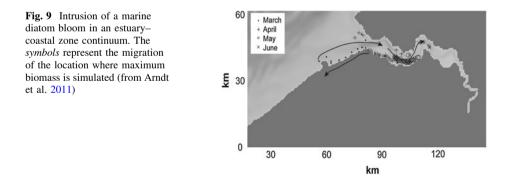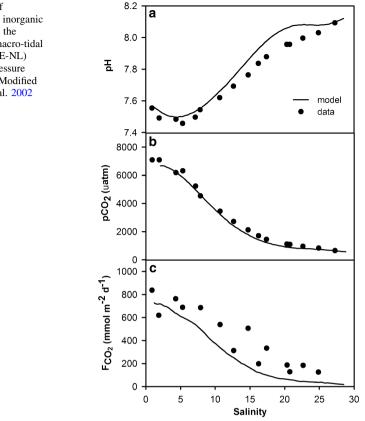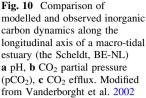
Fig. 8 Annual evolution of a dissolved silica budget. **a** riverine influx, **b** change in inventory, **c** silica consumption over the entire estuary, **d** residual export flux through estuarine mouth, **e** seasonally resolved estuarine budget. Each contribution is scaled to the yearly integrated riverine influx (820 10⁶ mol). Modified from Arndt et al. (2009)

Fig. 9 Intrusion of a marine diatom bloom in an estuary–coastal zone continuum. The *symbols* represent the migration of the location where maximum biomass is simulated (from Arndt et al. 2011)

in the biogeochemical dynamics (Fig. 9). In this transition zone, marked spatial concentration gradients develop and episodically lead to a reversal of material fluxes from the coast into the estuary (Arndt et al. 2011). During distinct episodes of the productive period, euryhaline coastal diatoms intrude far upstream into the saline estuary (Fig. 9), creating a strong CO_2 sink close to the estuarine mouth (Gypens et al. 2011). The diatom intrusion reduces the estuarine nutrient concentrations and export fluxes, thereby reinforcing the nutrient limitation in the coastal area. As a consequence, the estuarine filter does not operate independently from the processes in the coastal zone. The dynamic interplay

Fig. 10 Comparison of
modelled and observed inorganic
carbon dynamics along the
longitudinal axis of a macro-tidal
estuary (the Scheldt, BE-NL)
a pH, **b** CO_2 partial pressure
(pCO_2), **c** CO_2 efflux. Modified
from Vanderborght et al. 2002

between the two ecosystems and the intense process rates operating at their transition,
therefore, strongly support a continuum approach.

4.2.2 Disentangling the Biogeochemical Complexity: Models as Diagnostic Tools

RTMs can be used to disentangle the complex biogeochemical process interplay that
underlies system-wide biogeochemical indicators, such as NEM (e.g. Volta et al. 2013),
carbon and nutrient budgets (e.g. Soetaert and Herman 1995; Vanderborght et al. 2002),
filtering capacities (e.g. Arndt et al. 2009) or air–water CO_2 fluxes (Vanderborght et al.
2002; Hofmann et al. 2008a). For instance, a quantitative assessment of the air–estuarine
water CO_2 flux requires a consideration of all transport and reaction processes affecting
estuarine DIC, Alk and pH (see Sects. 3.1, 3.2), as well as temperature and ionic strength
effects on the dissociation constants of carbonate ions (Moek and Koene 1975; Cai and
Wang 1998; Regnier et al. 1997; Hofmann et al. 2008b).

   To the best of our knowledge, published modelling studies dedicated to estuarine CO_2
dynamics remain limited to the Scheldt estuary. Figure 10 compares RTM simulation
results of pH, partial pressure of CO_2 (pCO_2) and FCO_2 (Vanderborght et al. 2002) with
field observations from this highly heterotrophic system. The longitudinal profile of pH
exhibits a characteristic minimum at low salinity, which is mainly a consequence of

nitrification and, to a smaller extent, heterotrophic degradation and thermodynamic effects (Moek and Koene 1975; Frankignoulle et al. 1996; Regnier et al. 1997). The combined effects of CO_2-enriched river water, in situ degradation of organic matter and low pH, maintain pCO_2 values well above equilibrium with the atmosphere over the entire estuary. The RTM allows computing the daily-integrated CO_2 evasion fluxes driven by wind and currents and indicates that the estuarine system emits more than 200 tons of carbon per day (Vanderborght et al. 2002). Model results are compared to observed pH and pCO_2, as well as direct flux measurements performed using floating chambers (Frankignoulle et al. 1998), and the overall consistency between simulation results and observations can be considered as a robust test for the model. In particular, the estuarine pH is highly sensitive to many reaction processes and is thus a very good indicator of the model's ability to resolve the underlying biogeochemical dynamics. Small differences between measured and simulated FCO_2 fluxes likely result from the imperfect quantification of piston velocity in estuarine water.

The quantitative contribution of each biogeochemical process to variations in CO_2 concentration (and thus FCO_2) can be quantified through their respective effect on the change in DIC and Alk (Table 1). The rate of change in CO_2 concentration due to a given reaction ($dCO_2/dt|_{reaction}$) is calculated using an expression, which takes into account the buffering capacity of an ionic solution (e.g. Zeebe and Wolf-Gladrow 2001):

$$dCO_2/dt|_{reaction} = \left(\frac{dDIC/dt|_{reaction}}{D_s} - \frac{D_h}{D_s} \frac{dAlk/dt|_{reaction}}{A_h} \right) / \left(1 - \frac{D_h}{D_s} \frac{A_s}{A_h} \right) \qquad (1)$$

where D_S and A_s are the partial derivatives of DIC and Alk with respect to the CO_2 concentration at constant pH, respectively, and D_h and A_h are the partial derivatives of DIC and Alk with respect to pH at constant CO_2 concentration. Formulations and a detailed derivation for these partial derivatives are provided in Zeebe and Wolf-Gladrow (2001). For the CO_2 exchange flux, Eq. 1 reduces to the widely known Revelle equation (Revelle and Suess 1957) because alkalinity is constant. The above equation can be solved, for each process, at any given time and location. This approach allows quantifying the effect of individual biogeochemical processes on the CO_2 dynamics but ignores the comparatively smaller CO_2 changes due to advection and mixing (Hofmann et al. 2008b).

Here, the approach is used to quantify the relative contribution of different processes to the CO_2 dynamics in an idealized, funnel-shaped estuary for typical summer conditions representative of a temperate, Western European climate (Table 2). The RTM approach follows that of Regnier et al. (1997), Regnier and Steefel, (1999) and Vanderborght et al. (2002), but the model relies here on idealized geometries and generalized forcing conditions. In short, climate and hydrological forcings are extracted from monthly mean values for water temperature (World Ocean Atlas, http://www.nodc.noaa.gov/OC5/indprod.html), mean daily irradiance and photoperiods (Brock 1981), monthly averaged freshwater discharge (Fekete et al. 2002, 2010), and mean daily wind speed (CCMP project; Atlas et al. 2011). These forcings, derived from global databases, are available at a minimum resolution of 1° (Table 2). Water elevations at the estuarine mouth account for the dominant semi-diurnal tidal component M_2 with a constant tidal amplitude. The riverine inputs of carbon, nutrients and suspended particular matter (Table 3) are extracted from the global statistical model GlobalNEWS2 (Mayorga et al. 2010) and the Glorich database (Hartmann et al. 2011). Values represent a mean over all Western European watersheds that discharge through a tidal estuary (type 2 in the typology of Dürr et al. 2011). The lower boundary is located 20 km beyond the estuary mouth to minimize the marine influence (Table 3). The

Table 2 Climate forcings representative of temperate Western Europe used to constrain our simulations

Forcings	Value	Database spatial resolution
Water temperature (°C)	18	1°
Windspeed (m s^{-1})	2	0.25°
Mean solar radiation (μE m^{-2} s^{-1})	750	–
Photoperiod (h)	17	–

Table 3 Boundary conditions for biogeochemistry corresponding to the different simulations described in the text

	REF	POL (1–2)	PRIS (1–2)	Estuarine mouth
DIN (mmol m^{-3})	150	800	50	25
NH4/DIN	0.15	0.6	0.3	0.1
TOC (mmol m^{-3})	500	1000	300	0
Si (mmol m^{-3})	100	100	100	10
TSS (gr l^{-1})	0.07	0.07	0.07	0.03
O2 (mmol m^{-3})	200	100	300	220
P (mmol m^{-3})	7.5	10	5	0.1
DIC (mmol m^{-3})	3,160	3170–3375	3,045–2,837.5	2,209.8
ALK (mmol m^{-3})	3,000	3,000	3,000	2,476.4
pCO$_2$ (μatm)	4,205	5,000–9,000	2,000–367	367
pH	7.39	7.32–7.07	7.7–8.4	8.2

NB: ALK is constant, and pCO$_2$ is fixed. Other variables for the carbonate system are determined using those two values

parameter values of the biogeochemical reaction network and sediment parameters are adopted from Arndt et al. (2009) and Volta et al. (2013), respectively. These values are broadly consistent to other estimates reported for other tidal estuaries in Western Europe (Table in Online Resource).

Model results highlight the dominance of aerobic degradation in the total estuarine CO_2 production (~ 60 %). Denitrification plays, because of its low rates and strong buffering capacity, a much smaller role in total estuarine CO_2 production (~ 1 %). Nitrification exerts a significant influence on the CO_2 production and outgassing (~ 25 %) because it decreases Alk, lowers pH and, thus, shifts the equilibrium of DIC species towards CO_2. NPP generally promotes CO_2 uptake but is of minor significance (~ -5 %), due to the heterotrophic character of the simulated estuarine system. CO_2 outgassing decreases DIC without changing the alkalinity and hence promotes proton and CO_2 consumption, which counteracts its evasion. Overall, the CO_2 exchange through the air–water interface partly buffers the decrease in pH attributed to heterotrophic degradation and nitrification. The net rate of change in CO_2 (bold line in Fig. 11) indicates that the CO_2 concentration decreases all along the estuary, because the CO_2 outgassing exceeds its production by heterotrophic degradation and nitrification. In addition, the simulated spatially integrated DIC loss by outgassing (FCO$_2$) exceeds the production of DIC by NEM (Fig 11, inset). This result indicates that, in addition to nitrification (~ 25 %), another source largely attributable to the input of inorganic carbon from the river must contribute to the estuarine outgassing
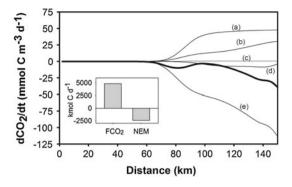
Fig. 11 Contribution of individual biogeochemical processes to estuarine atmosphere CO_2 flux for an idealized, funnel-shaped estuary. Positive values denote outgassing. *Thin lines*: *a*: aerobic degradation, *b*: nitrification, *c*: denitrification, *d*: NPP, *e*: gas dissolution. *Thick line*: net exchange rate. The inset shows the estuarine-integrated air–water CO_2 outgassing (FCO_2) and the NEM

($\sim$20 %). Such dynamics are supported by observations from rivers in the South-eastern USA, where high pCO_2 and large FCO_2 result from allochthonous inputs from tidally flooded salt marshes and groundwater (e.g. Cai and Wang 1998; Cai et al. 1999; Cai 2011).

4.3 Exploring Trends in Estuarine Biogeochemical Dynamics at Regional and Global Scales

The previous sections presented several examples of RTM applications to quantify and disentangle the complex process interplay that underlies the biogeochemical dynamics, air–water CO_2 fluxes and NEM along river–estuary–coastal zone continua at the local scale. However, RTMs can also be used to systematically explore the estuarine biogeochemical dynamics in a more general framework over a range of different, idealized estuarine geometries and a number of different environmental scenarios.

Here, we analyse the response of the biogeochemical indicators FCO_2, NEM and total C-filtering capacities to changes in estuarine geometry (funnel-shaped, mixed and prismatic; Table 4) for different environmental scenarios (polluted, reference and pristine; Table 5), again assuming typical Western European summer conditions. Steady-state simulations are performed for each estuarine geometry and environmental scenario. RTM simulations for the funnel-shaped estuary under reference conditions are already presented in Fig. 11 and discussed in Sect. 4.2.2.

Figure 12 a–d shows the longitudinal profiles of total heterotrophic degradation, nitrification and FCO_2 for the funnel-shaped and prismatic geometries under reference conditions for the set of kinetic constants reported in the literature (BASE). The sensitivity of these processes to changes in the interaction timescales between transport and biogeochemical processes is also shown, using rate constants for degradation and nitrification that are one order of magnitude smaller (SLOW). In addition, the response of biogeochemical reaction rates and FCO_2 to an increase in organic carbon, nutrient (Fig. 12e, f) and inorganic carbon (Fig. 12f) inputs (polluted scenario) is illustrated for the case of the funnel-shaped estuary.

Despite their very different geometries and, thus, hydrodynamic characteristics and residence times (Fig. 3), the funnel-shaped and prismatic estuaries reveal similar longitudinal rate and flux profiles (Fig. 12a–d). The highest reaction rates and FCO_2 are

Table 4 Generic estuarine geometries and corresponding hydrodynamic parameters

	Funnel shaped	Mixed	Prismatic
Length (km)	150	150	150
Width convergence length (km)	30	70	150
Depth (m)	7	7	7
Width at the mouth (km)	10	5	3
Discharge (m^3/s)	Q − (50)	Q ref (100)	Q ++ (300)
Tidal amplitude (M2) (m)	3.7	3	2.5

Table 5 Total C-filtering capacities expressed as percentage of the total riverine input for the baseline parametrization (BASE) and low kinetic constants parametrization (SLOW) for each estuarine geometry

	Funnel shaped		Mixed		Prismatic	
	BASE	SLOW	BASE	SLOW	BASE	SLOW
Ref.	31.3	28.3	29.6	22.5	25.0	10.2
POL1	58.3	52.1	57.6	41.4	52.8	20.2
POL2	60.7	54.7	61.0	45.6	56.0	25.0
PRIS1	23.5	21.8	21.1	17.2	16.5	7.2
PRIS2	18.9	16.6	16.9	11.3	11.9	1.1

simulated in the upper estuarine reaches. Both rates and fluxes decrease downstream as a consequence of organic matter and ammonium consumption by biogeochemical processes and dilution with seawater. In the funnel-shaped estuary, the rates become very low around 70 km and indicate that, due to the long residence time (~ 70 days), organic matter and ammonium are almost completely consumed in the upper estuarine reaches. The resulting decrease in reaction rates leads to a sharp decrease in FCO_2 in the same area. In the prismatic estuary, the shorter residence time (~ 8 days) is responsible for a slight downstream movement of the reaction front, which extends the reaction zone by about 10–20 km. Low reaction rates are nevertheless simulated in the lower estuary, indicating that the reduced species CH_2O (and ammonium) are also efficiently oxidized within the prismatic estuarine system. As a consequence, both estuaries are characterized by similar C-filtering capacities (Table 5).

A tenfold decrease in the rate constants for biogeochemical processes results in largely different longitudinal reaction rate profiles (Fig. 12a–d). In the funnel-shaped estuary, however, the reduction in reaction rate constants merely triggers an expansion of the organic matter degradation and nitrification zone by about 50 km (Fig. 12a), indicating that the long residence time of the system still allows for a complete consumption of the reactive species. In the prismatic estuary, on the other hand, the biogeochemical rates remain almost constant along the estuarine gradient (Fig. 12c). Here, the reduction in the rate constants increases the relative importance of the advective transport, which triggers a large export of organic matter (and ammonium) to the adjacent coastal ocean. In both estuaries, FCO_2 longitudinal profiles exhibit a rapid decrease due to the outgassing of saturated riverine waters to much lower values, resulting from a delicate balance between primary production (not shown) and the now reduced degradation and nitrification rates.
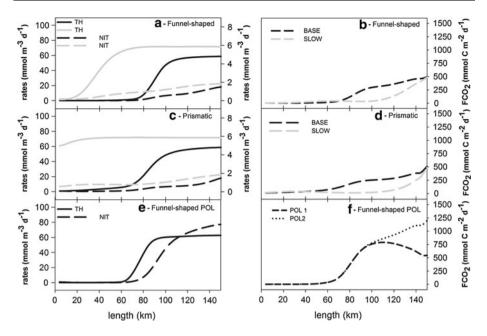
Fig. 12 Longitudinal profiles of total heterotrophic degradation (TH, aerobic degradation + nitrification) and nitrification rates (NIT), and corresponding FCO$_2$ along the estuarine gradient of a funnel-shaped estuary (**a**, **b**) and a prismatic estuary (**c**, **d**). SLOW indicates that organic matter degradation and nitrification kinetic constants are divided by 10 compared to BASE parameterization. **e** and **f** illustrates the effects of highly polluted systems (see Table 3 for description of the two pollution scenarios) on rates and fluxes for the funnel-shaped estuary

Overall, however, the C-filtering capacity of the prismatic estuary is much more sensitive (60 % decrease) to changes in reaction constants than the filtering capacity of the funnel-shaped system (10 % decrease). Simulation results thus emphasize the importance of the interaction timescales between biogeochemical and transport processes and, hence, between estuarine biogeochemistry and geometry.

Heavily polluted estuaries generally receive large ammonium and highly variable C loads. Therefore, riverine pollution may exert an important influence on the balance between heterotrophic degradation processes and nitrification, with potential implications for FCO$_2$. Fig. 12e, f illustrates the effect of pollution (increased organic carbon and ammonium loads) on total heterotrophic degradation and nitrification rates, as well as on estuarine CO$_2$ fluxes in the funnel-shaped estuary. Maximum degradation rates (Fig. 12e) remain similar to those predicted for the reference case (reflecting zero-order kinetics with respect to organic matter), but the zone of degradation expands by about ~25 km towards the mouth. Overall, the effect of this process on FCO$_2$ is moderate (Fig. 12f). Intense nitrification results in a pH decrease which triggers much higher FCO$_2$ (Fig. 12f) than in the reference case (Fig. 12a). The C-filtering capacities are thus significantly larger (Table 5) and are dominated by nitrification (see also Sect. 4.2.2). In the upper estuarine reaches, the pH drop due to nitrification leads to an initial increase in FCO$_2$, despite decreasing DIC concentrations (Fig. 12f). Further downstream, FCO$_2$ decreases in response to the downstream decrease in biogeochemical reaction rates and pCO$_2$, but the outgassing remains higher than in the reference case. An additional increase in riverine pCO$_2$ (larger DIC with constant alkalinity) supports an even larger outgassing fluxes within
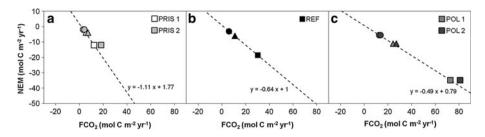
Fig. 13 NEM as a function of mean annual FCO_2 under pristine (PRIS 1 and PRIS 2, **a**), reference (REF, **b**) and polluted (POL 1 and POL 2, **c**) conditions (see Table 3). *Circles*, *triangles* and *squares* represent funnel-shaped, mixed-type and prismatic estuaries, respectively. The linear regression between NEM and FCO_2 is indicated for PRIS 1, REF and POL 1

the upper reaches (Fig. 12f) and, thus slightly higher C-filtering capacities (Table 5). Nevertheless, FCO_2 becomes similar for both pollution scenarios within a distance of circa 50 km, once most of the riverine supersaturated waters have outgassed within the estuary.

Table 5 complements the results shown in Fig. 12 and summarizes the results of our prognostic analysis of C-filtering capacities computed for all the estuarine types (funnel-shaped, mixed and prismatic) and environmental scenarios (pristine to heavily polluted conditions, Table 3). For all estuarine types, the C-filtering capacity increases from pristine to polluted conditions due to the increasing influence of nitrification on pH and CO_2 dynamics. Furthermore, the C-filtering capacity generally decreases with residence time, from funnel-shaped to mixed and then to prismatic estuarine types. Nevertheless, the effect of estuarine geometry and hydrodynamics strongly depends on the interaction timescales between biogeochemical reaction and transport processes. For the parameterization set using literature values, differences in filtering capacities across the different estuarine types do not exceed 10 %. However, the importance of estuarine geometry increases with the tenfold reduction in kinetic rate constants. Overall, lower kinetic constants induce significantly lower filtering capacities, but the relative decrease and its sensitivity to different environmental scenarios is much larger (>50 %) in the prismatic estuary than in the mixed (20–40 %) and funnel-shaped estuaries (<15 %) due to the short residence time (Table 5).

Figure 13 shows the relationship between estuarine FCO_2 and NEM for the three different estuarine geometries and the environmental scenarios analysed. Simulated FCO_2 and NEM fall within the range of globally observed values summarized by Laruelle et al. (2013) with mean values of 21.9 and -11.0 mol C m^{-2} $year^{-1}$, respectively. Simulation results show that for the reference conditions, the estuarine FCO_2 is mainly driven by heterotrophic processes and shows a strong linear correlation with NEM, in agreement with the results of Maher and Eyre (2012). The absolute magnitude of NEM and FCO_2 decrease from prismatic to mixed and to funnel-shaped because these variables correlate with the input fluxes and, thus, to the river discharges across estuarine types (Table 4). Figure 13 also shows that environmental conditions exert an important influence on the relationship between NEM and FCO_2. Under pristine conditions, the slope of the linear regression is steeper than under reference and polluted conditions. These findings emphasize that NEM is an important driver of FCO_2 in pristine systems. However, in polluted estuaries, the nitrification rates become increasingly more important and eventually support more than 50 % of the total CO_2 flux in the polluted scenario. In addition, higher riverine pCO_2 in the polluted scenario decreases further the slope of the regression lines, indicating that the contribution of supersaturated riverine waters becomes more important in the FCO_2 budget.

These results, albeit relying on a limited number of end-member cases, already highlight that the quantification of crucial biogeochemical processes and fluxes such as the FCO_2 results from a complex combination of factors, which can be identified and disentangled using RTMs with generic geometries and forcing conditions. Such a generic approach reduces data requirements and is numerically cost-efficient, but at the same time maintains the physical and biogeochemical complexity required to quantify estuarine biogeochemical dynamics (see Sects. 3.1, 3.2). Furthermore, it provides an objective, rational framework in which alternative simplification hypothesis and directions for meaningful upscaling strategies can be tested. In addition, the model approach can be combined with continuously growing global, high-resolution climatological, hydrological and environmental databases such as those used to design environmental scenarios for the presented set of prognostic RTM simulations. This combination offers promising avenues to assess the quantitative contribution of estuaries to global biogeochemical cycles and the response to climate change using mechanistically rooted upscaling strategies.

5 Conclusion and Outlook

Over the past few decades, increasingly complex reaction-transport modelling approaches have been applied to disentangle the interplay of physical, geochemical and biological processes that controls estuarine biogeochemical dynamics. These efforts have helped establish carbon and nutrient budgets and fluxes for many well-surveyed estuaries, at ever-increasing spatial and temporal resolution. Although clearly biased towards systems in industrialized countries, the modelling studies reveal that the estuarine bioreactor exerts a significant influence on land–ocean fluxes and is a relevant contributor to the atmospheric CO_2 budget. Yet, despite this widely recognized role, the global significance of estuaries for elemental cycles and climate remains frought with large uncertainties. This lack of quantitative understanding can be attributed mainly to the prohibitive computational cost required to simulate estuarine biogeochemical dynamics at the appropriate temporal and spatial scales, as well as the limited availability of comprehensive data sets that resolve the diversity of estuarine environments. Therefore, one of the biggest future challenges in estuarine biogeochemical research will be to develop suitable quantitative approaches that allow assessing the role of the estuarine biogeochemical reactor for global biogeochemical cycles and climate, as well as its response to climate and land-use changes at both a global scale and over climate relevant timescales. Here, we illustrated a data model approach that opens promising avenues in this direction, but also calls for:

- Comprehensive and Comparative Data Sets

The need for regionalization is evident because important controls of estuarine biogeochemical dynamics, such as temperature, watershed characteristics, organic matter inputs or pollution, vary geographically. Detailed local studies form the basis for the identification of global patterns. However, existing data sets are largely biased towards industrialized countries, while observations remain scarce for other regions. Future monitoring efforts should thus be strategically co-ordinated to fill these knowledge gaps.

- Continuum Approaches in Estuarine Research

A comprehensive assessment of the estuarine biogeochemical dynamics necessitates a continuum representation of the land–ocean interface, from the catchment to the coastal

zone. This is especially critical for reconstructing and forecasting the response of the estuarine filter to changes in land-use and climate.

- Integration Within Earth System Models

Earth system models (ESM) designed to study the coupled carbon cycle and climate lack an explicit representation of estuarine systems, mainly because of computational constraints. Therefore, upscaling strategies that allow incorporating the estuarine filter in ESMs at low computational costs need to be developed, in particular to separate the natural and anthropogenic contributions to the global estuarine carbon fluxes and their future response to climate and environmental change.

Our ability to understand the role of the land–ocean continuum for global biogeochemical cycles and climate will critically depend on a better quantitative understanding of the estuarine biogeochemical dynamics on a global scale.

References

Abril G, Riou SA, Etcheber H, Frankignoulle M, de Wit R, Middelburg JJ (2000) Transient, tidal time-scale, nitrogen transformations in an estuarine turbidity maximum-fluid mud system (The Gironde, South-West France). Estuar Coast Shelf Sci 50:703–715

Abril G, Nogueira M, Etcheber H, Cabeçadas G, Lemaire E, Brogueira MJ (2002) Behaviour of organic carbon in nine contrasting European estuaries. Estuar Coast Shelf Sci 54:241–262

Alin SR, Rasera MFFL, Salimon CI, Richey JE et al (2011) Physical controls on carbon dioxide transfer velocity and flux in low-gradient river systems and implications for regional carbon budgets. J Geophys Res Biogeosci 116. doi:10.1029/2010JG001398

Amann T, Weiss A, Hartmann J (2012) Carbon dynamics in the freshwater part of the Elbe estuary, Germany: implications of improving water quality. Estuar Coast Shelf Sci 107:112–121

Andersson AJ, Mackenzie FT (2004) Shallow-water oceans: a source or sink of atmospheric CO2? Front Ecol Environ 2:348–353

Arino O, Gross D, Ranera F, Bourg L, Leroy M, Bicheron P, Latham J, Di Gregorio A, Brockman C, Witt R, Defourny P, Vancutsem C, Herold M, Sambale J, Achard F, Durieux L, Plummer S, Weber J-L (2007) GlobCover: ESA service for global land cover from MERIS. In: Proceedings of the International Geoscience and Remote Sensing Symposium (IGARSS). IEEE International, Barcelona, pp 2412–2415

Arndt S, Regnier P (2007) A model for the benthic-pelagic coupling of silica in estuarine ecosystem: sensitivity analysis and system scale simulation. Biogeosciences 4:331–352

Arndt S, Vanderborght JP, Regnier P (2007) Diatom growth response to physical forcing in a macro tidal estuary: coupling hydrodynamics, sediment transport, and biogeochemistry. J Geophys Res 112. doi:10.1029/2006JC003581

Arndt S, Regnier P, Vanderborght JP (2009) Seasonally-resolved nutrient filtering capacities and export fluxes in a macrotidal estuary. J Mar Syst 78:42–58

Arndt S, Lacroix G, Gypens N, Regnier P, Lancelot C (2011) Nutrient dynamics and phytoplankton development along an estuary-coastal zone continuum: a model study. J Mar Syst 84:49–66

Arndt S, Jørgensen BB, LaRowe DE, Middelburg JJ, Pancost R, Regnier P (2013) Quantifying the degradation of organic matter in marine sediments: a review and synthesis. Earth-Sci Rev 123:53–86

Aston SR (1983) Silicon geochemistry and biogeochemistry. Academic Press, London

Atlas R, Hoffman RN, Ardizzone J, Leidner SM, Jusem JC, Smith DK, Gombos D (2011) A cross-calibrated multiplatform ocean surface wind velocity product for meteorological and oceanographic applications. Bull Am Meteor Soc 92:157–174

Baklouti M, Chevalier C, Bouvy M, Corbin D, Pagano M, Troussellier M, Arfi R (2011) A study of plankton dynamics under osmotic stress in the Senegal River Estuary, West Africa, using a 3D mechanistic model. Ecol Model 222:2704–2721

Benoit P, Gratton Y, Mucci A (2006) Modeling of dissolved oxygen levels in the bottom waters of the Lower St. Lawrence Estuary: coupling of benthic and pelagic processes. Mar Chem 102:13–32

Benson BB, Krause D Jr (1984) The concentration and isotopic fractionation of oxygen dissolved in freshwater and seawater in equilibrium with the atmosphere. Limnol Oceanogr 29:620–637

Beusen AHW, Dekkers ALM, Bouwman AF, Ludwig W, Harrison J (2005) Estimation of global river transport of sediments and associated particulate C, N and P. Global Biogeochem Cycles 19. doi: 10.1029/2005GB002453

Bianchi TS (2007) Biogeochemistry of estuaries. Oxford University Press, Oxford

Bianchi TS (2011) The role of terrestrial derived organic carbon in the coastal ocean: a changing paradigm and priming effect. Proc Natl Acad Sci 108:19473–19481

Billen G (1975) Nitrification in the Scheldt Estuary (Belgium and The Netherlands). Estuar Coast Mar Sci 3:79–89

Billen G, Somville M, De Becker E, Servais P (1985) A nitrogen budget of the Scheldt hydrographical basin. Neth J Sea Res 19:223–230

Billen G, Lancelot C, Maybeck M (1991) N, P and Si retention along the aquatic continuum from land to ocean. In: Mantoura RFC, Martin JM, Wollast R (ed) Ocean margin processes in global change. Dahlem workshop reports, Wiley, pp 19–44

Billen G, Garnier J, Ficht A, Cun C (2001) Modeling the response of water quality in the Seine River estuary to human activity in its watershed over the last 50 years. Estuaries 24:977–993

Billen G, Thieu V, Garnier J, Silvestre M (2009) Modelling the N cascade in regional watersheds: the case study of the Seine, Somme and Scheldt rivers. Agric Ecosyst Environ 133:234–246

Borges AV (2005) Do we have enough pieces of the jigsaw to integrate CO2 fluxes in the coastal ocean? Estuaries 28:3–27

Borges AV, Abril G (2011) Carbon dioxide and methane dynamics in estuaries. Treatise Estuar Coast Sci 5:119–161

Borges AV, Frankignoulle M (2002) Aspects of dissolved inorganic carbon dynamics in the upwelling system on the Galician coast. J Mar Syst 32:181–198

Borges AV, Delille B, Schiettecatte LS, Gazeau F, Abril G, Frankignoulle M (2004) Gas transfer velocities of CO2 in three European estuaries (Renders Fjord, Scheldt, and Thames). Limnol Oceanog 49:1630–1641

Borges AV, Delille B, Frankignoulle M (2005) Budgeting sinks and sources of CO2 in the coastal ocean: diversity of ecosystems counts. Geophys Res Lett 32:L14601. doi:10.1029/2005GL023053

Bowden KF (1963) The mixing processes in a tidal estuary. Int J Air Water Pollut 7:343–356

Boyle E, Collier R, Dengler AT, Edmond JM, Ng AC, Stallard RF (1974) On the chemical mass-balance in estuaries. Geochim Cosmochim Acta 38:1719–1728

Boynton WR, Garber JH, Summers R, Kemp WM (1995) Inputs, transformations and transport of nitrogen and phosphorus in Chesapeake Bay and selected tributaries. Estuaries 18:285–314

Brion N, Billen G (1998) A re-assessment of H14CO−3 incorporation method for measuring autotrophic nitrification and its use to estimate nitrifying biomasses. Rev Sci Eau 11:283–302

Brock T (1981) Calculating solar radiation for ecological studies. Ecol Model 14:1–19

Cai WJ (2011) Estuarine and coastal ocean carbon paradox: CO2 sinks or sites of terrestrial carbon incineration. Annu Rev Mar Sci 3:123–145

Cai WJ, Wang Y (1998) The chemistry, fluxes and sources of carbon dioxide in the estuarine waters of the Satilla and Altamaha Rivers, Georgia. Limnol Oceanogr 43:657–668

Cai WJ, Pomeroy LR, Moran MA, Wang Y (1999) Oxygen and carbon dioxide mass balance in the estuarine/intertidal marsh complex of five rivers in the Southeastern US. Limnol Oceanogr 44:639–649

Cai WJ, Dai M, Wang Y, Zhai W, Huang T, Chen S et al (2004) The biogeochemistry of inorganic carbon and nutrients in the Pearl River estuary and the adjacent Northern South China Sea. Cont Shelf Res 24:1301–1319

Cai WJ, Guo X, Chen CTA, Dai M, Zhang L, Zhai W, Lohrenz SE, Yin K et al (2008) A comparative overview of weathering intensity and HCO3-flux of the world's major rivers with emphasis on the Changjiang, Huanghe, Zhujiang (Pearl) and Mississippi Rivers. Cont Shelf Res 28:1538–1549

Canuel EA, Cammer SS, McIntosh A, Pondell C (2012) Climate change impact on the organic carbon cycle at the land–ocean interface. Annu Rev Earth Planet Sci 40:685–711

Cerco CF (2000) Phytoplankton kinetics in the Chesapeake Bay eutrophication model. Water Qual Ecosyst Model 1:5–49

Cerco CF, Cole T (1993) Three-dimensional eutrophication model of Chesapeake Bay. J Environ Eng 119:10061025

Cerco CF, Noel MR (2004) Process-based primary production modelling in Chesapeake Bay. Mar Ecol Prog Ser 282:45–58

Cerco CF, Tillman D, Hagy JD (2010) Coupling and comparing a spatially- and temporally-detailed eutrophication model with and ecosystem network model: an initial application to Chesapeake Bay. Environ Model Softw 25:562–572

Chen CTA, Liu KK, MacDonald R (2003) Continental margin exchanges. In: Fasham MJR (ed) Ocean biogeochemistry: a synthesis of the joint global ocean flux study (JGOFS). Springer, Berlin, pp 53–97

Cloern JE (1996) Phytoplankton bloom dynamics in coastal ecosystems: a review with some general lessons from sustained investigation of San Francisco Bay, California. Rev Geophys 34:127–168

Cloern JE (1999) The relative importance of light and nutrient limitation of phytoplankton growth: a simple index of coastal ecosystem sensitivity to nutrient enrichment. Aquat Ecol 33:3–16

Cloern JE (2001) Our evolving conceptual model of the coastal eutrophication problem. Mar Ecol Prog Ser 210:223–253

Cloern JE, Alpine BE, Cole RL, Wong J, Arthur JF, Ball MD (1983) River discharge controls phytoplankton dynamics in the northern San Francisco Bay estuary. Estuar Coast Shelf Sci 16:415–429

Compton J, Mallinson D, Glenn CR, Filippelli G, Follmi K, Shields G, Zanin Y (2000) Variations in the global phosphorus cycle. Marine authigenesis: from global to microbial. SEPM Special Publication 66:21–33

Conley DJ (1997) Riverine contribution of biogenic silica to the oceanic silica budget. Limnol Oceanogr 42:774–777

Corine Land Cover data set. http://www.eea.europa.eu

Cugier P, Billen G, Guillaud JF, Menesguen A (2005) Modelling the eutrophication of the Seine Bight (France) under historical, present and future riverine nutrient loading. J Hydrol 304:381–396

Dai M, Guo X, Zhai W, Yuan L, Wang B, Wang L, Cai P, Tang T, Cai WJ (2006) Oxygen depletion in the upper reach of the Pearl River estuary during a winter drought. Mar Chem 102:159–169

Dai M, Wang L, Guo X, Zhai W, Li Q, He B, Kao SJ (2008) Nitrification and inorganic nitrogen distribution in a large perturbed river/estuarine system: the Pearl River Estuary, China. Biogeosciences 5:1227–1244

Dalrymple RW, Zaitlin BA, Boyd R (1992) Estuarine facies models: conceptual basis and stratigraphic implications. J Sediment Petrol 62:1130–1146

de Leeuw JW, Largeau C (1993) A review of macromolecular organic compounds that comprise living organism and their role in kerogen, coal and petroleum formation. In: Engel MH, Macko SA (eds) Organic geochemistry principles and applications. Plenum Publishing Corp, New York, pp 23–72

DeMaster DJ (1981) The supply and accumulation of silica in the marine environment. Geochim Cosmochim Acta 45:1715–1732

Desmit X, Vanderborght JP, Regnier P, Wollast R (2005) Control of phytoplankton production by physical forcing in a strongly tidal, well-mixed estuary. Biogeosciences 2:205–218

Dettman EH (2001) Effect of water residence time on annual export and denitrification of nitrogen in estuaries: a model analysis. Estuaries 24:481–490

Ducklow HW, McAllister SL (2004) The biogeochemistry of carbon dioxide in the coastal oceans. In: Robinson AR, Brink K (eds) The Sea. Harvard University Press, Cambridge, pp 193–225

Dürr HH, Laruelle GG, van Kempen CM, Slomp CP, Meybeck M, Middelkoop H (2011) Worldwide typology of nearshore coastal systems: defining the estuarine filter of river inputs to the oceans. Estuaries Coasts 34:441–458

Dyer KR (1995) Sediment transport in estuaries. In: Perillo GME (ed) Geomorphology and sedimentology of estuaries. Elsevier, Amsterdam, pp 423–449

Dyer KR (2001) Suspended sediment transport in the Humber estuary. In: Huntley DA, Leeks GJL, Walling DE (eds) Land–Ocean Interaction: Measuring and Modelling Fluxes from River Basins to Coastal Seas. IAWQ, London, pp 169–183

Elliott M, McLusky DS (2002) The need for definitions in understanding estuaries. Estuar Coast Shelf Sci 55:815–827

Even S, Billen G, Bacq N, Thery S, Ruelland D, Garnier J, Cugier P, Poulin M, Blanc S, Lamy F, Paffoni C (2007a) New tools for modelling water quality of hydrosystems: an application in the Seine River basin in the frame of the Water Framework Directive. Sci Total Environ 375:274–291

Even S, Thouvenin B, Bacq N, Billen G, Garnier J, Guezennec L, Blanc S, Ficht A, Le Hir P (2007b) An integrated modelling approach to forecast the impact of human pressure in the Seine estuary. Hydrobiol 588:13–29

Eyre BD (2000) A regional evaluation of nutrient transformation and phytoplankton growth in nine river dominated sub-tropical East Australian estuaries. Mar Ecol Prog Ser 205:61–83

Eyre BD, Balls PW (1999) A comparative study of nutrient processes along the salinity gradient of tropical and temperate estuaries. Estuar Coast 22:313–326

Eyre BD, McKee L (2002) Carbon, nitrogen and phosphorus budgets for a shallow sub-tropical coastal embayment (Moreton Bay, Australia). Limnol Oceanogr 47:1043–1055

Falkowski P, Scholes RJ, Boyle E, Canadell J, Canfield D, Elser J, Gruber N, Hibbard K, Högberg P, Linder S, Mackenzie FT et al (2000) The Global Carbon Cycle: A test of our Knowledge of Earth as a System. Science 290. doi: 10.1126/science2905490291

Fekete BM, Vörösmarty CJ, Grabs W (2002) High-resolution fields of global runoff combining observed river discharge and simulated water balances. Glob Biogeochem Cycles 16:815–827

Fekete BM, Wisser D, Kroeze C, Mayorga E, Bouwman L et al (2010) Millennium Ecosystem Assessment scenario drivers (1970–2050): climate and hydrological alterations. Glob Biogeochem Cycles 24:815–827

Fisher TR, Hardings LW Jr, Stanley DW, Ward LG (1988) Phytoplankton, nutrients, and turbidity in the Chesapeake, Delaware, and Hudson estuaries. Estuar Coast Shelf Sci 27:61–93

Follows MJ, Dutkiewicz S, Ito T (2006) On the solution of the carbonate system in ocean biogeochemistry models. Ocean Model 12:290–301

Frankignoulle M, Bourge I, Wollast R (1996) Atmospheric CO2 fluxes in a highly polluted estuary (The Scheldt). Limnol Oceanogr 41:365–369

Frankignoulle M, Abril G, Borges A, Bourge I, Canon C, Delille B, Libert E, Theate JM (1998) Carbon dioxide emission from European estuaries. Science 282:434–436

Friedrichs CT, Aubrey DG (1988) Non-linear tidal distortion in shallow well mixed estuaries: a synthesis. Estuar Coast Shelf Sci 27:521–545

Frossard E, Brossard M, Hedley MJ, Mertherell A (1995) Reactions controlling the cycling of P in soils. In: Tiessen H (ed) Phosphorus cycling in terrestrial and aquatic ecosystems: a global perspective. SCOPE/Wiley, New York, pp 107–137

Garnier J, Billen G, Costa M (1995) Seasonal succession of diatoms and Chlorophyceae in the drainage network of the Seine River: observations and modeling. Limnol Oceanogr 40:750–765

Garnier J, Billen G, Cebron A (2007) Modelling nitrogen transformations in the lower Seine river and estuary (France): impact of waste release on oxygenation and N2O emission. Hydrobiologia 588:291–302

Garnier J, Billen G, Even S, Etcheber H, Servais P (2008) Organic matter dynamics and budgets in the turbidity maximum zone of the Seine Estuary (France). Estuar Coast Shelf Sci 77:150–162

Gattuso JP, Frankignoulle M, Wollast R (1998) Carbon and carbonate metabolism in coastal aquatic ecosystems. Annu Rev Ecol Syst 29:405–434

Gazeau F, Smith SV, Gentili B, Frankignoulle M, Gattuso JP (2004) The European coastal zone: characterization and first assessment of ecosystem metabolism. Estuar Coast Shelf Sci 60:673–694

Gazeau F, Gattuso JP, Middelburg JJ, Brion N, Schiettecatte LS (2005) Planktonic and whole system metabolism in a nutrient-rich estuary (the Scheldt estuary). Estuaries 28:868–883

GESAMP (1987) Land/Sea boundary flux of contaminants: contributions from rivers. Rep Stud GESAMP

Giese BS, Jay DA (1989) Modelling tidal energetics of the Columbia River estuary. Estuar Coast Shelf Sci 29:549–571

Gordon DC Jr, Boudreau PR, Mann KH, Ong JE et al (1996) LOICZ biogeochemical modelling guidelines. LOICZ reports and studies no 5, pp 1–96

Guan W, Wong L, Xu D (2001) Modeling nitrogen and phosphorus cycles and dissolved oxygen in the Zhujiang estuary. II. Model results. Acta Oceanol Sin 20:505–514

Guéguen C, Laodong G, Deli W, Noriyuki T, Chin-Chang H (2006) Chemical characteristics and origin of dissolved organic matter in the Yukon River. Biogeochemistry 77:139–155

Gypens N, Lacroix G, Lancelot C, Borges AV (2011) Seasonal and inter-annual variability of air-sea CO2 fluxes and seawater carbonate chemistry in the Southern North Sea. Prog Oceanogr 88:59–77

Gypens N, Delhez E, Vanhoutte-Brunier A, Burton S, Thieu V, Passy P, Liu Y, Callens J, Rousseau V, Lancelot C (2012) Modelling phytoplankton succession and nutrient transfer along the Scheldt estuary (Belgium, The Netherlands). J Mar Syst. doi:10.1016/j.jmarsys.2012.10.006

Haag D, Kaupenjohann M (2000) Biogeochemical models in the environmental science. Int J Phylosophy Chem 6:117–142

Hanley N, Faichney R, Munro A, Shortle JS (1998) Economic and environmental modelling for pollution control in an estuary. J Environ Manag 52:211–225

Harding LWJ, Meeson BW, Fisher TRJ (1986) Phytoplankton production in two east coast estuaries: photosynthesis-light functions and patterns of carbon assimilation in Chesapeake and Delaware Bays. Estuar Coast Shelf Sci 23:773–806

Hartmann J, Kempe S (2008) What is the maximum potential for CO2 sequestration by stimulated weathering on the global scale? Naturwissenschaften 95:1159–1164

Hartmann J, Lauerwald R, Moosdorf N, Amann T, Weiss A (2011) GLORICH: GLobal River and estuary CHemical database. ASLO, San Juan

Hedges JI, Keil RG (1999) Organic geochemical perspectives on estuarine processes: sorption reactions and consequences. Mar Chem 65:55–65

Hedges JI, Eglinton G, Hatcher PG, Kirchman DL et al (2000) The molecularly-uncharacterized component of nonliving organic matter in natural environments. Org Geochem 31:945–958

Heip C, Herman PMJ (1995) Major biological processes in European tidal estuaries: a synthesis of the JEEP-92 Project. Hydrobiologia 311:1–7

Hofmann AF, Soetaert K, Middelburg JJ (2008a) Present nitrogen and carbon dynamics in the Scheldt estuary using a novel 1-D model. Biogeosciences 5:981–1006

Hofmann AF, Meysman FJR, Soetaert K, Middelburg JJ (2008b) A step-by-step procedure for pH model construction in aquatic systems. Biogeosciences 5:227–251

Horrevoets AC, Savenije HHG, Schuurman JN, Graas S (2004) The influence of river discharge on tidal damping in alluvial estuaries. J Hydrol 294:213–228

Howarth RW, Jensen H, Marino R, Postma H (1995) Transport to and processing of P in near-shore and oceanic waters. In: Tiessen H (ed) Phosphorus in the global environment transfers, cycles and management SCOPE 54. Wiley, Chichester, pp 323–345

Jay DA, Giese BS, Sherwood CR (1990) Energetics and sedimentary processes in the Columbia River estuary. Prog Oceanogr 25:157–174

Jiang LQ, Cai WJ, Wang Y (2008) A comparative study of carbon dioxide degassing in river- and marine-dominated estuaries. Limnol Oceanogr 53:2603–2615

Kaul LW, Froelich PN (1984) Modeling estuarine nutrient geochemistry in a simple system. Geochim Cosmochim Acta 48:1417–1433

Keeney-Kennicutt WL, Presley BJ (1986) The geochemistry of trace metals in the Brazos river estuary. Estuar Coast Shelf Sci 22:459–477

Keil RG, Mayer LM, Quay PD, Richey JE, Hedges JI (1997) Loss of organic matter from riverine particles in deltas. Geochim Cosmochim Acta 61:1507–1511

Ketchum BH (1955) Distribution of coliform bacteria and other pollutant in tidal estuaries. Sewage Ind Wastes 27:1288–1296

Kim S, Cerco CF (2003) Hydrodynamic and eutrophication model of the Chester River estuary and the Eastern Bay estuary.Oceanol 45:67–80

Krom MD, Berner RA (1980) Adsorption of phosphate in anoxic marine sediments. Limnol Oceanogr 25:797–806

Lancelot C, Muylaert K (2011) Trends in estuarine phytoplankton ecology. Treatise Estuar Coast Sci 7:5–15

Lancelot C, Veth C, Mathot S (1991) Modelling ice-edge phytoplankton bloom in the Scotia-Weddell sea sector of the Southern Ocean during spring 1988. J Mar Syst 2:333–346

Lancelot C, Hannon E, Becquevort S, Veth C, de Baar HJW (2000) Modelling phytoplankton blooms and carbon export production in the Southern Ocean: dominant controls by light and iron in the Atlantic sector in Austral spring 1992. Deep-Sea Res I 47:1621–1662

Langdon C (1988) On the causes of interspecific differences in the growth-irradiance relationship for phytoplankton. II. A general review. J Phytoplankton Res 10:1291–1312

Laruelle GG, Regnier P, Ragueneau O, Kempa M, Moriceau B, Ni Longphuirt S, Leynaert A, Thouzeau G, Chauvaud L (2009a) Benthic-pelagic coupling and the seasonal silica cycle in the Bay of Brest (France): new insights from a coupled physical-biological model. Mar Ecol Prog Ser 385:15–32

Laruelle GG, Roubeix P, Sferratore A, Brodherr B, Ciuffa D, Conley DJ, Dürr HH, Garnier J, Lancelot C, Le Thi Phuong Q, Meunier JD, Meybeck M, Michalopoulos P, Moriceau B, Ní Longphuirt S, Loucaides S, Papush L, Presti M, Ragueneau O, Regnier PAG, Saccone L, Slomp CP, Spiteri C, Van Cappellen P (2009b) The global biogeochemical cycle of silicon: role of the land–ocean transition and response to anthropogenic perturbation. Glob Biogeochem Cycles 23. doi: 10.01029/2008GB003267

Laruelle GG, Dürr HH, Slomp CP, Borges AV (2010) Evaluation of sinks and sources of CO2 in the global coastal ocean using a spatially-explicit typology of estuaries and continental shelves. Geophys Res Lett 37:1–6

Laruelle GG, Dürr HH, Lauerwald R, Hartmann J, Slomp CP, Goossens N, Regnier PAG (2013) Global multi-scale segmentation of continental and coastal waters from the watersheds to the continental margins. Hydrol Earth Syst Sci 17:2029–2051

Lauerwald R, Hartmann J, Ludwig W, Moosdorf N (2012) Assessing the non-conservative fluvial fluxes of dissolved organic carbon in North America. J Geophys Res. doi: 10.1029/2011JG001820

Lee DI, Parl CK, Cho HS (2005) Ecological modeling for water quality management of Kwangyang Bay, Korea. J Environ Manag 74:327–337

Lefort S, Gratton Y, Mucci A, Dadou I, Gilbert D (2012) Hypoxia in the Lower St. Lawrence Estuary: how physics controls spatial patterns. J Geophys Res 117:1–14

Lewitus AJ, Kana TM (1995) Light respiration in six estuarine phytoplankton species: contrasts under photoautotrophic and mixotrophic growth conditions. J Phycol 31:754–761

Lichtner PC, Steefel CI, Oelkers EH (1996) Reactive transport in porous media. Reviews in mineralogy, vol 34. The mineralogical society of America, Washington

Lin J, Xie L, Pietrafesa LJ, Ramus JS, Paerl HW (2007) Water quality gradients across Albemarle-Pamlico estuarine system: seasonal variations and model applications. J Coast Res 23:213–229

Lin J, Xie L, Pietrafesa LJ, Xu H, Woods W, Mallin MA, Durako MJ (2008) Water quality responses to simulated flow and nutrient reductions in the Cape Fear River Estuary and adjacent coastal region, North Carolina. Ecol Model 212:200–217

Lionard M, Muylaert K, Van Gansbeke D, Vyverman W (2005) Influence of changes in salinity and light intensity on growth of phytoplankton communities from the Scheldt river and estuary (Belgium/The Netherlands). Hydrobiologia 540:105–115

Liss PS (1976) Conservative and non-conservative behavior of dissolved constituents during estuarine mixing. In: Burton JD, Liss PS (eds) Estuarine chemistry. Academic Press, London, pp 93–130

Macedo MF, Duarte P (2006) Phytoplankton production modelling in three marine ecosystems: static versus dynamic approach. Ecol Model 190:299–316

Mackenzie FT (2013) Sediments, Diagenesis, and Sedimentary Rocks. Volume 7 of Treatise on Geochemistry. Elsevier, New York

Mackenzie FT, Lerman A, Andersson AJ (2004) Past and present of sediment and carbon biogeochemical cycling models. Biogeoscience 1:11–32

Mackenzie FT, Andersson AJ, Lerman A, Ver LM (2005) Boundary exchanges in the global costal margin: implications for the organic and inorganic carbon cycles. In: Robinson AR, Brink KH (eds) The sea. Harvard University Press, Cambridge, pp 193–225

Mackenzie FT, Lerman A, DeCarlo EH (2011) Coupled C, N, P and O biogeochemical cycling at the land–ocean interface. Treatise Estuar Coast Sci 5:317–342

Maher DT, Eyre BD (2012) Carbon budget for three autotrophic Australian estuaries: Implications for global estimates of the coastal air-water CO_2 flux. Glob Biogeochem Cycles. doi: 10.1029/2011GB004075

Margvelashvili N, Robson B, Sakov P, Webster IT, Parslow J, Herzfeld M, Andrewartha J (2003) Numerical modelling of hydrodynamics, sediment transport and biogeochemistry in the Fitzroy Estuary. Tech Rep 9. Cooperative Research Centre for Coastal Zone Estuary and Waterway Management

Mayorga E, Seitzinger SP, Harrison JA, Dumont E, Beusen AHW, Bouwman AF, Fekete BM, Kroeze C, Van Drecht G (2010) Global nutrient export from WaterSheds 2 (NEWS 2): model development and implementation. Environ Model Softw 25:837–853

Meybeck M (1993) Riverine transport of atmospheric carbon: sources, global typology and budget. Water Air Soil Poll 70:443–463

Middelburg JJ, Herman PMJ (2007) Organic matter processing in tidal estuaries. Mar Chem 106:127–147

Mills GL, Quinn JG (1984) Dissolved copper and copper-organic complexes in the Narrangasett Bat estuary. Mar Chem 15:151–172

Moek W, Koene B (1975) Chemistry of dissolved inorganic carbon in estuarine and coastal brackish waters. Esuar Coast Shelf Sci 3:325–336

Moosdorf N, Hartmann J, Lauerwald R, Hagedom B, Kempe S (2011) Atmospheric CO_2 consumption by chemical weathering in North America. Geochim Cosmochim Acta 75:7829–7854

Mortazavi B, Iverson RL, Huang W, Lewis GF, Caffrey JM (2000) Nitrogen budgets of Apalachicola Bay, Florida, a bar-built estuary in the northeastern Gulf of Mexico. Mar Ecol Prog Ser 195:1–14

Mulholland PJ (1997) Dissolved organic matter concentration and flux in streams. J North Am Benthol Soc 16:131–141

Muylaert K, Sabbe K, Vyverman W (2009) Changes in phytoplankton diversity and community composition along the salinity gradient of the Scheldt estuary (Belgium/The Netherlands). Estuar Coast Shelf Sci 82:335–340

Nedwell DB, Trimmer M (1996) Nitrogen fluxes through the upper estuary of the Great Ouse, England: the role of the bottom sediments. Mar Ecol Prog Ser 142:273–286

Nielsen K, Nielsen LP, Rasmussen P (1995) Estuarine nitrogen retention independently estimated by the denitrification rate and mass balance methods: a study of Norsminde Fjord, Denmark. Mar Ecol Prog Ser 119:275–283

Nixon SW, Ammerman JW, Atkinson LP et al (1996) The fate of nitrogen and phosphorus at the land–sea margin of the North Atlantic Ocean. Biogeochemistry 35:141–180

Nowicki BL, Requintina E, Van Keuren D, Kelly JR (1997) Nitrogen losses through sediment denitrification in Boston Harbor and Massachusetts Bay. Estuaries 20:626–639

O'Connor DJ, Dobbins WE (1956) Mechanism of reaeration in natural streams. J Sanit Eng Divis ASCE 82(SA6):1–30

Odum HT (1956) Primary production in flowing waters. Limnol Oceanogr 1:102–117

Officer CB (1980) Box models revisited. In: Hamilton P, MacDonald KB (eds) Estuarine and wetlands processes. Plenum Press, New York, pp 65–114

Officer CB, Lynch DR (1981) Dynamics of mixing in estuaries. Estuar Coast Shelf Sci 12:525–533

Officer C, Biggs J, Taft J, Cronin L (1984) Chesapeake Bay anoxia: origin, development, and significance. Sci 223:22–27

O'Kane JP (1980) Estuarine water quality management. Pitman, London

O'Kane JP, Regnier P (2003) A mathematically transparent low-pass filter for tidal estuaries. Estuar Coast Shelf Sci 57:593–603

Paerl HW, Pinckney JL, Fear JM, Peierls BL (1998) Ecosystem responses to internal and watershed organic matter loading: consequences for hypoxia in the eutrophying Neuse River Estuary, North Carolina, USA. Mar Ecol Prog Ser 166:17–25

Paerl HW, Valdes LM, Peierls BL, Adolf JE, Harding LW Jr (2006) Anthropogenic and climatic influences on the eutrophication of large estuarine ecosystems. Limnol Oceanogr 51:448–462

Pallud C, Van Cappelen P (2006) Kinetics of microbial sulfate reduction in estuarine sediments. Geochim Cosmochim Acta 70:1148–1162

Parker BB (1991) The relative importance of the various nonlinear mechanisms in a wide range of tidal interactions (a review). In: Parker BB (ed) Tidal hydrodynamics. Wiley, New York, pp 237–268

Paytan A, McLaughlin K (2007) The oceanic phosphorus cycle. Chem Rev 107(563):576

Pritchard DW (1974) Dispersion and flushing of pollutants in estuaries. J Hydraul Div 95:115–124

Qin YC, Weng HW (2006) Silicon release and its speciation distribution in the superficial sediments of the Pearl River Estuary, China. Estuar Coast Shelf Sci 67:433–440

Quinton JN, Govers G, Van Oost K, Bardgett RD (2010) The impact of agricultural soil erosion on biogeochemical cycling. Nat Geosci 3:311–314

Rabalais NN, Turner RE (2001) Coastal Hypoxia: Consequences for Living Resources and Ecosystems. Coast Estuar Stud 58. doi: 10.1029/CE058

Rabouille C, Mackenzie FT, Ver LM (2001) Influence of the human perturbation on carbon, nitrogen, and oxygen biogeochemical cycles in the global coastal ocean. Geochim Cosmochim Acta 65:3615–3641

Raymond PA, Cole JJ (2001) Gas exchange in rivers and estuaries: choosing a gas transfer velocity. Estuaries 24:312–317

Raymond PA, Oh NH, Turner RE, Broussard W (2008) Anthropogenically enhanced fluxes of water and carbon from the Mississippi River. Nature 451:449–452

Regnier P, Steefel CI (1999) A high resolution estimate of the inorganic nitrogen flux from the Scheldt estuary to the coastal North Sea during a nitrogen limited algal bloom, spring 1995. Geochim Cosmochim Acta 63:1359–1374

Regnier P, Wollast R, Steefel CI (1997) Long-term fluxes of reactive species in macrotidal estuaries: estimates from a fully transient, multicomponent reaction-transport model. Mar Chem 58:127–145

Regnier P, Mouchet A, Wollast R, Ronday F (1998) A discussion of methods for estimating residual fluxes in strong tidal estuaries. Cont Shelf Res 18:1543–1571

Regnier P, Vanderborght JP, Steefel CI, O'Kane JP (2002) Modeling complex multi-component reactive-transport systems: towards a simulation environment based on the concept of a Knowledge Base. Appl Math Model 26:913–927

Regnier P, Arndt S, Dale AW, LaRowe DE, Mogollon J, Van Cappellen P (2011) Advances in the biogeochemical modeling of the marine methane cycle. Earth Sci Rev 106:105–130

Regnier P, Friedlingstein P, Ciais P, Mackenzie FT, Gruber N, Janssens I, Laruelle GG, Lauerwald R, Luyssaert S, Andersson AJ, Arndt S, Arnosti C, Borges AV, Dale AW, Gallego-Sala A, Goddéris Y, Goossens N, Hartmann J, Heinze C, Ilyina T, Joos F, LaRowe DE, Leifeld J, Meysman FJR, Munhoven G, Raymond PA, Spahni R, Suntharalingam P, Thullner M (2013) Anthropogenic perturbation of the carbon fluxes from land to ocean. Nat Geosci 6(8):597–607

Revelle R, Suess HE (1957) Carbon dioxide exchange between atmosphere and ocean and the question of an increase of atmospheric CO2 during the past decades. Tellus 9:18–27

Robson BJ, Hamilton DP (2004) Three-dimensional modelling of a microcystis bloom event in the Swan River estuary, Western Australia. Ecol Model 174:203–222

Robson BJ, Bukaveckas PA, Hamilton DP (2008) Modelling and mass balance assessment of nutrient retention in a seasonally-owing estuary (Swan River Estuary, Western Australia). Estuar Coast Shelf Sci 76:282–292

Savenije HHG (1992) Rapid assessment technique for salt intrusion in alluvial estuaries. IHE report series 27, Delft

Savenije HHG (2005) Salinity and tides in alluvial estuaries, 1st edn. Elsevier, Amsterdam

Scavia D, Kelly ELA, Hagy JD III (2006) A simple model for forecasting the effects of nitrogen loads on Chesapeake Bay hypoxia. Estuaries Coast 29:674–684

Schroeder F (1997) Water quality in the Elbe estuary: significance of different processes for the oxygen deficit at Hamburg. Environ Model Assess 2:73–82

Seitzinger SP (1988) Denitrification in freshwater and coastal marine ecosystems: ecological and geochemical significance. Limnol Oceanogr 33:702–724

Seitzinger SP, Harrison JA, Dumont E, Beusen AHW, Bouwman AF (2005) Sources and delivery of carbon, nitrogen, and phosphorous to the coastal zone: an overview of Global Nutrient Export from Watersheds (NEWS) models and their application. Glob Biogeochem Cycles 19:75–89

Shen J (2006) Optimal estimation of parameters for a estuarine eutrophication model. Ecol Model 191:521–537

Shiller AM (1996) The effect of recycling traps and upwelling on estuarine chemical flux estimates. Geochim Cosmochim Acta 55:3241–3251

Smith SV, Hollibaugh JT (1993) Coastal metabolism and the oceanic organic carbon balance. Rev Geophys 31:75–89

Soetaert K, Herman PMJ (1995) Nitrogen dynamics in the Westerschelde estuary (S.W. Netherlands) estimated by means of the ecosystem model MOSES. Hydrobiologia 311:225–246

Soetaert K, Middelburg JJ, Heip C (2006) Long-term change in dissolved inorganic nutrients in the heterotrophic Scheldt estuary (Belgium, The Netherlands). Limnol Oceanogr 51:409–423

Sommerfield CK, Wong KC (2011) Mechanisms of sediment flux and turbidity maintenance in the Delaware Estuary. J Geophys Res 116. doi:10.1029/2010JC006462

Spiteri C, Van Cappellen P, Regnier P (2008) Surface complexation effects on phosphate adsorption to ferric iron oxyhydroxides along pH and salinity gradients in estuaries and coastal aquifers. Geochim Cosmochim Acta 72:3431–3445

Stommel H (1953) Computation of pollution in a vertically mixed estuary. Sewage Ind Wastes 25:1065–1071

Struyf E, Van Damme S, Gribsholt B, Meire P (2005) Freshwater marshes as dissolved silica recyclers in an estuarine environment (Schelde estuary, Belgium). Hydrobiologia 540:69–77

Tappin AD (2002) An examination of the fluxes of nitrogen and phosphorus in temperate and tropical estuaries: current estimates and uncertainties. Estuar Coast Shelf Sci 55:885–901

Tappin AD, Harris JRW, Uncles RJ (2003) The fluxes and transformations of suspended particles, carbon and nitrogen in the Humber estuarine system (UK) from 1994 to 1996: results from an integrated observation and modelling study. Sci Total Environ 314–316:665–713

Thieu V, Mayorga E, Billen G, Garnier J (2010) Sub-regional and downscaled-global scenarios of nutrient transfer in river basins: the seine-Scheldt-Somme case study. Special issue "Past and Future Trends in Nutrient Export from Global Watersheds and Impacts on Water Quality and Eutrophication". Global Biogeochem Cycles 24:1–15

Thieu V, Billen G, Garnier J, Benoît M (2011) Nitrogen cycling in a hypothetical scenario of generalized organic agriculture in the Seine, Somme and Scheldt watersheds. Reg Environ Change 11:359–370

Thullner M, Regnier P, Van Cappellen P (2007) Modeling microbially induced carbon degradation in redox-stratified subsurface environments: concepts and open questions. Geomicrobiol J 24. doi:10.1080/01490450701459275

Trimmer M, Nedwell DB, Sivyer DB, Malcom SJ (1998) Nitrogen fluxes through the lower estuary of the river Great Ouse, England: the role of the bottom sediments. Mar Ecol Prog Ser 163:109–124

Uncles RJ, Jordan MB (1980) One-dimensional representation of residual currents in the Severn Estuary and associated observations. Estuar Coast Mar Sci 10:39–60

Uncles RJ, Radford PJ (1980) Seasonal and spring-neap tidal dependence of axial dispersion coefficients in the Severn: a wide, vertically mixed estuary. J Fluid Mech 98:703–726

Uncles RJ, Stephens JA (1999) Suspended sediment fluxes in the tidal Ouse, UK. J Hydrol Process 13:1167–1179

van Beusekom JEE, de Jonge VN (1998) Retention of phosphorus and nitrogen in the Ems estuary. Estuaries 21:527–539

Van Cappellen P, Wang Y (1996) Cycling of iron and manganese in surface sediments: a general theory for the coupled transport and reaction of carbon, oxygen, nitrogen, sulfur, iron and manganese. Am J Sci 296:197–243

van der Zee C, Roevros N, Chou L (2007) Phosphorus speciation, transformation and retention in the Scheldt estuary (Belgium/The Netherlands) from the freshwater tidal limits to the North Sea. Mar Chem 106:76–91

Vanderborght JP, Wollast R, Loijens M, Regnier P (2002) Application of a transport-reaction model to the estimation of biogas fluxes in the Scheldt estuary. Biogeochem 59:207–237

Vanderborght JP, Folmer I, Aguilera DR, Uhrenholdt T, Regnier P (2007) Reactive-transport modelling of a river-estuarine-coastal zone system: application to the Scheldt estuary. Mar Chem 106:92–110

Ver LMB, Mackenzie FT, Lerman A (1999) Carbon cycle in the coastal zone: effects of global perturbations and change in the past three centuries. Chem Geol 159:283–304

Volta C, Arndt S, Savenije HHG, Laruelle GG, Regnier P (2013) C-GEM (v 1.0): a new, cost-efficient biogeochemical model for estuaries and its application to a funnel-shaped system. Geosci Model Dev Discuss 6:5645–5709

Wanninkhof R (1992) Relationship between wind speed and gas exchange over the ocean. J Geophys Res 97:7373–7382

Webster IT, Smith SV, Parslow J (2000) Implications of spatial and temporal variation for biogeochemical budgets of estuaries. J Phys Oceanogr 12:112–115

Weiss RF, Price BA (1980) Nitrous oxide solubility in water and seawater. Mar Chem 8:347–359

Wild-Allen K, Skerratt J, Rizwi F, Parslow J (2009) Derwent estuary biogeochemical model: Technical report. CSIRO Mar Atmos Res

Wollast R (1983) Interaction in estuaries and coastal waters. In: Bolin B, Cook RB (eds) The major biogeochemical cycles and their interactions. Wiley, SCOPE, pp 385–407

Wollast R (1998) Evaluation and comparison of the global carbon cycle in the coastal zone and in the open ocean. In: Brink KH, Robinson AR (eds) The major biogeochemical cycles and their interactions. Wiley-Interscience, New York

Wollast R, Peters JJ (1978) Biogeochemical properties of an estuarine system: the river Scheldt. Biogeochemistry of estuarine sediments: In: Proceedings of a UNESCO/SCOR workshop held in Melreux, Begium (1976)

Wulff F, Stigebrandt A, Rahm L (1990) Nutrient dynamics of the Baltic Sea. Ambio 19:126–133

Wulff F, Eyre BD, Johnstone R (2011) Nitrogen versus phosphorus limitation in a subtropical coastal embayment (Moreton Bay; Australia): implications for management. Ecol Model 222:120–130

World Ocean Atlas. http://www.nodc.noaa.gov/OC5/indprod.html

Yeats PA (1993) Input of metals to the North Atlantic from two large Canadian estuaries. Mar Chem 43:201–209

Zeebe RE, Wolf-Gladrow D (2001) CO2 in seawater: equilibrium, kinetics, isotopes. Elsevier, Amsterdam

Zhai W, Dai M, Cai W, Wang Y, Wang Z (2005) High partial pressure of CO2 and its maintaining mechanism in a subtropical estuary: the Pearl River estuary, China. Mar Chem 93:21–32

Zhang H, Li S (2010) Effects of physical and biochemical processes on the dissolved oxygen budget for the Pearl River Estuary during summer. J Mar Syst 79:65–88